Growth and Characterisation of Boron Rich Nanomaterials.

Steffan John Lea

Submitted for the Degree of
Master of Science

Department of Physics
University of York

January 2010

Abstract

In this study nanomaterials are grown in a solid state reaction at 1300°C of boron, barium oxide and iron(II/III)oxide powders in an argon atmosphere. The nanomaterials are shown to be grown via vapour based method by growing the nanomaterials on a separate silicon wafer that has been sputtered with iron and placed downstream of the powders in the flow of argon. An area of the silicon wafer is kept free of iron by using a mask when sputtering the wafer. When nanomaterials are grown, the masked area remains free of nanomaterials. This shows that the presence of iron is vital for the nucleation of the nanomaterials and also indicates the possibility of growing these nanomaterials on targeted sites.

The nanomaterials produced are examined and it is found that we have a presence of amorphous, crystalline and multiple twinned nanowires. The evidence collected suggests that $\sim 70\%$ of the nanowires are twinned. The single crystal nanowires can be identified as boron carbide by comparing to diffraction pattern simulations of a boron carbide unit cell. The twinned diffraction pattern is shown to be due to different segments of the nanowire being in different diffraction condition by using Dark Field imaging. The Twinned wires are also shown to have at least four segments in a cyclic [001] twinning orientation in simultaneous diffraction condition by comparing to a twinned structure constructed from simulations. Elemental analysis using Electron Energy Loss Spectroscopy and Energy Dispersive X-ray shows that the composition of the nanomaterials is mainly boron and carbon.

The role of the iron layer on the wafer is investigated to see how varying the thickness will affect the nanomaterials grown. It is successfully shown that an increase in the thickness of the iron layer results in a greater density of nanomaterials. However there is no great variation in the average diameter of the nanomaterials produced.

The absence of a visible signal for iron in the Elemental analysis of nanostructure covered silicon wafer shows that the amount of iron in the sample has decreased during the reaction. However iron is found in small amounts in droplet structures at the tips of nanomaterials this is different to work done on a similar system at 1100°C. This suggests that the role of the iron in the growth of these nanomaterials at this temperature is not yet understood. However this work has confirmed that the iron is essential for the nucleation of the nanomaterials, but post nucleation growth that was previously assumed to be a conventional VLS growth may switch to an oxide assisted growth mode.

Contents

List of Figures

List of Tables

Declarations

I declare that the work presented in this thesis, except where otherwise stated, is based on my own research and has not been submitted previously for a degree in this or any other university. Parts of the work reported in this thesis have been published in:

Zhiyang Yu, Steffan Lea, Jun Yuan, "CVD growth of boron-rich nanostructures", *Accepted for EMAG 2009* ,

Signed

Your Name

Acknowledgements

Ambition is critical.

Dylan Thomas

I would like to thank all those that helped me complete this project. A special thanks goes to Jun Yuan who's supervision and helpful discussions have helped to steer this project to its conclusion.

I would like to thank the technicians Dave Coulthard, Richard Armitage and Neil Johnson for helping to obtain and assemble equipment and keep it in working order.

Brent Wilkinson, and the rest of the workshop technicians for fabricating and helping to design the pellet die and for not being to angry when asked to repair it when broken.

A special thank you to Ian Wright at the Nanocentre for doing a brilliant job in keeping the microscopes working, for teaching me to use many of the tools used during my work and pointing me in the right direction when I was stuck.

Thank you to the secretaries especially Jo Crawford for all the free food.

Thanks to the Occupants of my office and many of the other residents of the physics department for keeping me sane and in high spirits during my time here.

A final thank you to my parents who have been supportive at all times and have always encouraged me to aim high.

Chapter 1

Introduction

Equipped with his five senses, man explores the universe around him and calls the adventure Science

Edwin Powell Hubble

1.1 The topic of this research.

This thesis aims to deal with the synthesis of boron rich nanomaterials. Specifically this work will deal with a five fold twinned nanowire morphology made of boron carbide (B_4C). The work aims to further the understanding of a complex system and take steps to optimise the system so that an improvement in efficiency is obtained. This will also lead to further study of a novel structure that (i.e. forbidden) does not exist in bulk materials. We will vary the parameters of the growth conditions and deduce any trends that are present as a result of these variations.

1.2 An introduction to Nanomaterials.

In materials science a nanomaterial is a material that has constituents which are of nanoscale dimensions [1]. This means that the material measures between 1 and 100 nm in at least one dimension. A vast variety of different types of nanomaterials have been observed through the years from simple nanoparticles to complex structures that self assemble to form structures that look similar to trees.

Because of the small size of nanomaterials the physics that govern the behavior of materials changes. This makes nanomaterials a very important class of materials to study. Nanomaterials provide a means to study how material properties such as electric transport [2], field emission [3] and the Young's modulus [4] vary when their nanoscale properties are compared to their properties in bulk materials. They also contribute greatly to the understanding of basic concepts in science. Nanomaterials have been successfully applied to technological roles, for example logic gates have been fabricated using semiconductor nanowire junctions [5], and have been shown to be capable of basic computation [5]. Here is a brief description of a few nanostructures significant to this work.

A nanowire is a structure that is confined to the nanoscale in two dimensions and has a diameter of nanometers [1]. Nanowires are of a particular interest to those interested in building small scale nanodevices because they may potentially be used as building blocks [6].

Nanotubes are like wires but have a hollow core. They tend to grow with smaller diameters than wires [7].

Nanobelts [8], Nanoplatelets [9] or Nanoribbons [10] are only confined to the nanoscale in a single direction. This makes them long and wide but thin, like a belt or a ribbon.

1.3 Problems with Nanomaterials research.

In order to do research on nanomaterials it is often desirable to accurately position them to perform analysis or incorporate them into a device (e.g. the work done by Huang *et al* [5]). Because nanowires are small there are obstacles to easily manipulating them. High precision tools are required to handle such small objects.

When nanostructures are grown in large volumes they may intertwine with each other, this is inconvenient if the nanostructures are to be isolated for use or analysis. One way to avoid this problem is to directly grow the nanowire on the site where it will ultimately be used. However growing a single nanowire poses its own problems also.

Another aspect of nanowire growth under lively debate is the proposed growth mode. In the literature there is a wide variety of proposed growth paths. Some of the proposals can be applied successfully to many different materials, however then there are materials to which none of the existing proposals seem to

apply and a variation of a growth mode is often proposed. This shows that there are many factors that need to be taken into account to fully describe and understand the growth process.

One of the obstacles to solving the argument about how a particular nanowire is grown is that until recently it has not been possible to observe nanomaterials while they are growing. The growth methods initially proposed were educated guesses taking into account the products of the reaction and the energetics. Recently growth of nanostructures has been observed directly inside specially adapted microscopes [11]. This development in technology has helped but it is still very new and not very widespread and many questions remain unanswered.

1.4 An introduction to boron rich materials.

Boron is a lightweight non-metallic material with unique physical properties. With a high melting point of 2300°C [7], and a hardness comparable to that of diamond and excellent mechanical and thermal properties [7]. Boron rich compounds are particularly suited to certain applications such as lightweight high temperature high strength materials as well as micro-electronic, nuclear and medical applications [12]. In addition to these properties several unique morphologies of boron rich nanostructures have been reported. Boron is used extensively in the electronics industry as a dopant for semiconductors. The boron can donate a hole to the semiconducting material because it has fewer valance electrons than the semiconductor. This in turn improves the conduction of the semiconductor [13].

1.5 Nanowires of boron rich materials.

In general nanowires have very different properties from the bulk material. As an example metal nanowires exhibit higher strength when compared with their bulk materials. The difference in properties is attributed to a decreased defect density resulting from the reduced dimensions of the nanomaterials [14].

Because boron has a high melting temperature and is extremely hard in its bulk form it is likely that nanomaterials with these desirable properties could be produced. These types of materials potentially have been proposed as reinforcement for a plastic matrix to create lightweight high strength materials.

The high temperature of these wires also has applications, however boron is highly contaminating so is not suitable for applications such as high temperature containers for chemical reactions.

Chapter 2

Background.

Men Love to wonder, and that is the seed of Science

Ralph Waldo Emerson

2.1 General concepts of material growth.

In science and technology it is often desirable to produce materials that have specific properties. One of the dominant factors determining the properties of a material is the formation of the desired material from a vapour, a solid, or a liquid precursor. The material grows from a nucleus which is formed as the concentration of the atoms becomes sufficiently high. These newly formed nuclei act as seeds for further growth [11].

Several different methods have been developed for material growth. Each method has a varying level of control that can be exploited depending on the type of nanowire that is desired. Here commonly used methods of growing materials are covered.

2.1.1 Vapour phase growth.

The first method of growing materials that will be covered in this work relies on the material arriving at the growth site in a vapour phase. The vapour phase can be in the form of pure atoms, or molecules containing the desired atoms. Vapour based growth is convenient because the vapour is easily transported to the growth site and is easily separated from the other reaction products once the reaction has finished. Vapour phase growth can be further divided into physical and chemical depositions.

2.1.1.1 Physical Vapour Deposition.

Physical Vapour Deposition (PVD) is used to deposit thin films of a material on a surface by condensing the material from its vapour form [15]. The deposition is purely physical i.e. simply heating, and no chemical reaction is required to release the atoms desired for deposition. The vaporised material can be produced by many methods. Commonly used techniques include heating [16] and laser ablation [17].

2.1.1.2 Chemical Vapour Deposition.

Chemical Vapour Deposition (CVD) can also used to produce thin films on a surface [18]. The process works by exposing the growth site to a precursor gas which reacts and decomposes on the surface depositing the material on to the site of growth. This process is different to PVD due to the chemical reaction required to liberate the desired atoms for deposition.

2.1.2 Solid media reaction.

Another method of growing nanostructures is through a reaction between solids [19]. The reaction occurs when the materials are heated in the absence of solvents. The materials usually in powder form must be well mixed in order to increase the yield. This type of reaction may contain a liquid phase as the materials are heated and can sometimes be referred to as a Solid Liquid Solid (SLS) reaction. This method when used for growing nanostructures is not ideal, because there is a lot of bulk material in the reaction product as well as the nanostructures.

2.1.3 Liquid phase growth.

Material growth can be facilitated through a liquid medium [20]. The atoms in a liquid suspension can be deposited onto the surface of a solid. Important factors in Liquid phase growth are the temperature, the viscosity of the liquid and the amount of liquid.

2.2 The mechanics of nanowire growth.

Since the first observations nanostructures there has been interest in the way in which these structures are synthesised. Materials such as nanowires are impor-

tant for the study of how the electrical and optical properties of materials vary on the nanoscale when compared to bulk materials. Such one dimensional materials are also attractive as they would be easily adapted to be incorporated into devices such as logic gates [5].

One of the crucial factors in the synthesis of nanowires is the control of composition, size and morphology. Once the material has reached the growth site, the material is incorporated into the nanostructure. There are various mechanisms that allow for the growth of nanostructures.

2.2.1 Vapour Solid.

In the Vapour Solid (VS) path, the material is absorbed directly into the solid from the vapour [11]. This is a simple reaction that allows the growth of nanostructures. It is useful because there is no need for a catalyst that may affect the purity of the end product. This method can appear to be slow and inefficient when compared to other catalysed methods.

2.2.2 Vapour Liquid Solid.

In the Vapour Liquid Solid (VLS) path, the material from the vapour is firstly absorbed into a catalytic liquid metal alloy. As the alloy saturates with the material it is then precipitated onto the interface between the liquid alloy and the solid nanostructure [11]. This method was proposed by Wagner and appears to be widely accepted and applied to many different cases. The growth is explained by looking at the phase diagram between the liquid and the solid. The boron and iron form a liquid alloy when the temperature is higher than the eutectic point $\sim 1100^{\circ}$C and as the percentage of the boron in the sample increases a phase boundary is crossed and now a solid is formed at the solid liquid interface. The main evidence for this proposed method was the observation of metal droplets at the end of the nanowires, but in situ observations of Ge nanowires have been reported in TEM[11]. Controlling the size of the droplet allows for control of the diameter of the nanowire [21]. Generally a quicker than VS, however if a nanowire has grown via VLS the catalyst is only found at the tip of the wire, VS growth can still occur at the sides of the wire unless they are pacified.

2.2.3 Oxide Assisted Growth.

Oxide Assisted Growth (OAG) is similar to VLS but instead of the metal catalyst, an oxide forms the liquid interface [11]. The growth of the structure is aided by the presence of the oxide. The oxide has a catalytic role in the growth of nanostructures. This mode of growth is less well understood than VLS and was proposed by a group studying the growth of silicon nanowires.

2.3 Boron rich nanowires.

Ever since the observation of nanomaterials there has been a great interest in understanding their properties both structural and mechanical. A variety of different structures have been synthesised using a variety of different materials. The properties of a nanostructure can depend on the method that was used to grow it. This section will review the methods used to produce boron rich nanomaterials and in particular boron rich nanowires and boron carbide.

In order to produce nanostructures they must be grown by forming nuclei. These nuclei are the seeds that crystals will grow from. A nucleus will grow in all directions but if there is a preferred direction of growth that is energetically favorable it will form into a wire. There are many methods that have been developed to grow nanowires. Each method gives a varying degree of control over the parameters of the nanowire.

2.3.1 Existing methods of boron rich nanowire growth.

Now that some of the growth modes have been discussed we will pay more attention to our specific case of boron rich nanowires. There have been many reports of boron rich nanowires being produced and by different techniques.

Amorphous nanowires have been grown on a large scale without a catalyst by Cao *et al* [22]. Radio frequency magnetron sputtering of a boron target in a protective argon atmosphere was used to grow boron nanowires on a silicon substrate. The boron nanowires produced were well ordered with an uniform length and diameter. The work also demonstrated that at ambient temperature these wires were stable under pressure.

Also reporting a high density of self orientated amorphous nanowires is Wang *et al* [23]. This technique also used radio frequency magnetron sputtering on a silicon substrate but with a target made of a mixture of boron and boron oxide. They are of the opinion that the growth of these wires is not described

by methods such as CVD and propose a variant on the oxide assisted growth as a likely alternative.

Amorphous boron rich nanowires have also been grown by Guo *et al* using a CVD process [16]. A nickel covered silicon substrate was heated to 900 Celsius and reacted with a diborane gas precursor. They claim that a catalyst is not necessary for the growth the boron rich nanowires in their study due to the lack of preferential nucleation sites. But they do state that CVD growth is present in the system.

Another CVD process using a diboran precursor gas with a silicon substrate is detailed by Yang *et al* [24]. However the catalyst used in the reaction is gold. The boron nanowires synthesised have a variety of diameters and morphologies. Most of the nanowires grown were amorphous. They successfully demonstrate a size dependency of the thickness of the wires on the thickness of the catalyst film.

Single crystalline boron nanowires are also reported by Zhang *et al* [17]. The nanowires are grown by laser ablation in an argon atmosphere. The work demonstrates the growth with a variation of catalysts with varying success. They propose that the growth is VLS based due to the nanostructures only growing in the downstream direction in the argon flow.

Single crystalline boron carbide nanowires have also been produced by Ma *et al* [25]. The samples were powder based and were grown at 1650°C in a high frequency induction furnace. The growth is explained by a Vapour Solid reaction.

Twinned nanowires have also been grown using a diborane gas by Otten *et al* [26]. The gas was passed over NiB powder on an alumina substrate in a furnace at 1100°C. They propose that CVD growth is present in this reaction.

Cao *et al* report the synthesis of boron suboxide nanomaterials from a solid state reaction [27]. The nanomaterials are produced from a mixture of very pure CaO, B and Fe_3O_4, the composition of the powder mixture is varied and the compositions that produce nanomaterials are noted in figure 2.1. From looking at the figure it can clearly be seen that when no iron is present no nanomaterials are produced. The same is true for CaO. The experimental procedure involved milling the powders for two hours in alcohol, then forming a tablet in a pressure cell with glycerine as a binding agent. The tablet was heated in an argon atmosphere to 1450°C and held at this temperature for 4 hours. Chemical analysis of the nanomaterials shows that they are composed of boron and oxygen in a ratio of 6:1. Diffraction techniques were also used to confirm a B_6O composition. The author indicates that although the growth

mechanism is complex and poorly understood, he believes that it is related to the conventional VLS. It is also observed that the Iron is incorporated into the center of some nanomaterials.

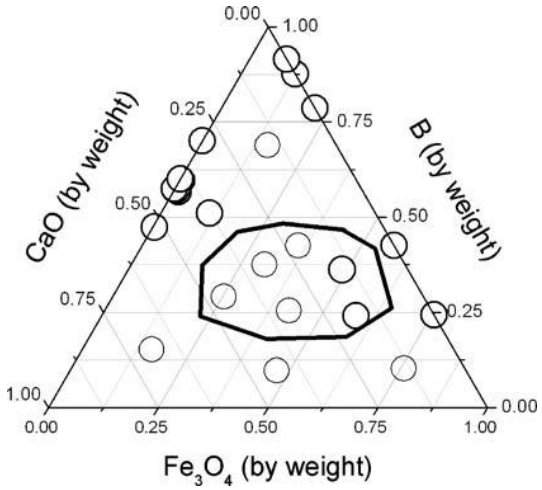

Figure 2.1: Adapted from Cao *et al*. J Electroceram (2006) 17:817.
Composition of powder mixture for work done by Cao *et al*. Nanomaterials are only produced in the circled area.

Jiang *et al* present a cyclic twinned nanowire [28]. The nanowires were synthesised in a solid state reaction of boron, calcium oxide and magnetite powders that had been milled and pressed into pellets. The pellets were heated to 1400°C for 2 hours in a flowing argon atmosphere. Electron Energy Loss Spectroscopy (EELS) and Diffraction methods are used to confirm that the nanowires are probably B_6O. It is reported that there are traces of silicon in the wires, this is attributed to the purity of the boron powder. The five fold twinning structure is confirmed by systematically tilting the nanowire to two highly symmetric crystallographic orientations that are 18° apart and comparing to simulations of a five fold structure. The author suggests that nanomaterials with a similar structure should be observable in related boron rich compounds as they have a very similar closed packing structure.

Using the same method as the previous author Fu *et al* have grown boron carbide five fold twinned nanowires [29]. The cyclically twinned nanowires were synthesised in a solid state reaction at 1100°C using a pellet made from compacted Fe_3O_4, BaO and B powders. The work shows that VLS growth is responsible for the growth of the nanowires as demonstrated in figure 2.2. These images show that the iron exists as a droplet structure at the top of the nanowire and is consistent with previous observations of typical VLS systems such as that described by Cui *et al* [21]

In a similar system but at 1300°C Jiang demonstrates in his PhD thesis that nanowire can grow without the iron being present [30]. His work in figure 2.3

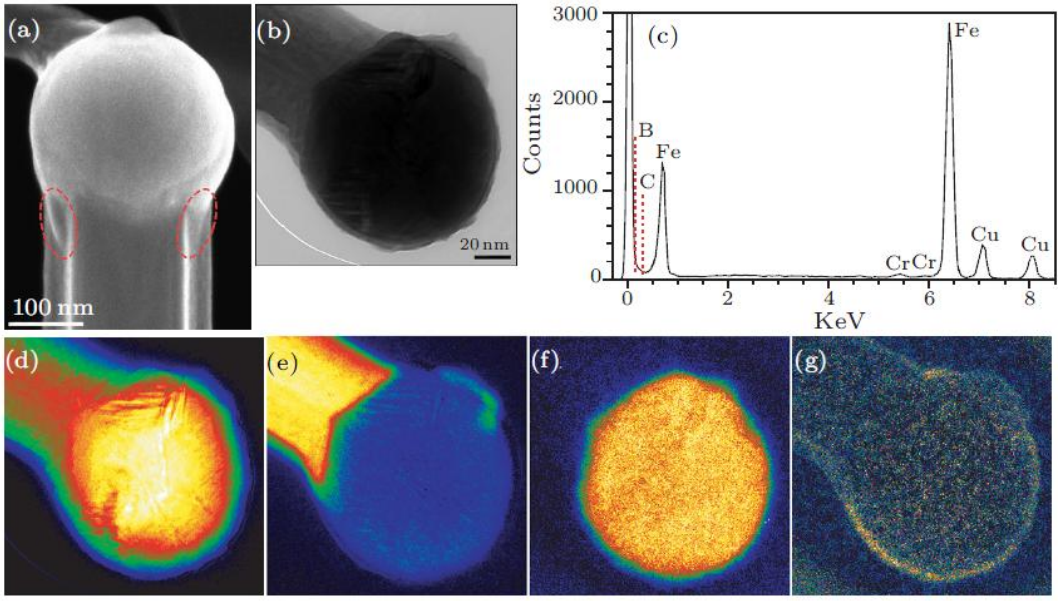

Figure 2.2: Adapted from Fu *et al*. CHIN. PHYS. LETT.(2009) 26,8:086110. (a) A catalytic particle under SEM shows well wettability with boron carbide nanowires highlighted by dashed red circles. (b) A catalytic particle consist of 26.22 at.% B, 6.65 at.% C and 67.12 at.% Fe identified by EDS quantification (c), the Cr and Cu elements in EDS spectrum are from the copper grid. Its thickness mapping is shown in (d). The boron, iron and surface oxygen elemental mapping are shown in (e), (f) and (g), respectively.

shows EELS scans of a droplet structure that contains no iron. Further evidence is supplied by High Angle Annular Dark Field (HAADF) imaging, because this technique is sensitive to the atomic number, the iron appears bright in the image compared to boron. We can clearly see in figure 2.3 that the trail of iron has ended but the nanowire has continued to grow along it. These observations throw doubt on the growth being a conventional VLS system as the growth can continue without the iron being present.

2.4 What is twinning and a fivefold structure.

In the previous section it has been mentioned that twinned nanomaterials have been produced. Twinning is common in crystalline materials and is described by the *International Tables for Crystallography*, Volume D: Physical Properties of Crystals [31]. Twins may form as a result of erroneously attaching atoms or molecules to a growing crystal such that two crystals appear to be growing out of or into each other. The boundary that forms between is known as the twin boundary. Twinning can occur as single incidences or they can be repeated [14]. The scientific community is aware of two distinct types of repeated twinning, Lamellar twinning where the twining planes are parallel and the twins

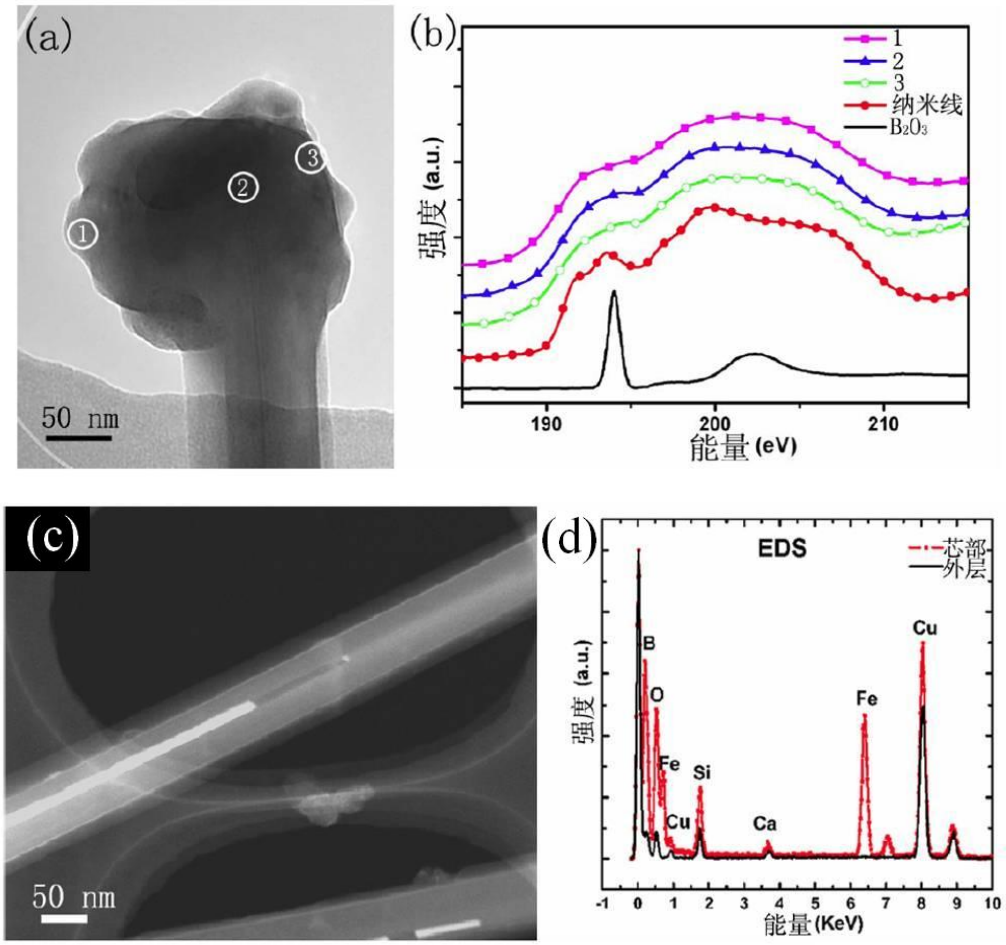

Figure 2.3: Adapted from Jun Jiang. PhD Thesis, Tsinghua University, 2007 Feature of the head of nanowire a). EELS charictirisation (b). HAADF image for nanowire with iron Fe core (c). Components of the core and outer part of the nanowire (d).

repeat continuously one after the other. The other is cyclic twinning, where all twin planes share a common axis and the angle between two twinning planes must be an integer of 360°. The five fold structure can exist in any crystalline material that allows twinning on alternate coplanar twin planes that are separated by an angle of about $2\pi/5$. The arrangement of the twin boundaries for a five fold twinned structure is shown in figure 2.4. Five fold twinning is often found in many elements especially transition metals, some lanthanide and in a few of the metallic group II, III, IV elements with an FCC crystal lattice [14].

Properties of bulk materials greatly depend on the microstructure such as crystalinity, defects and grain boundaries. However at the nanoscale methods of strengthening by incorporating impurities are ineffective due to the finite size of the nanomaterials. Therefore exploiting the microstructure is the most efficient method of varying the strength of the material.

Work done on five fold silver nanowires shows that the twinned nature of the

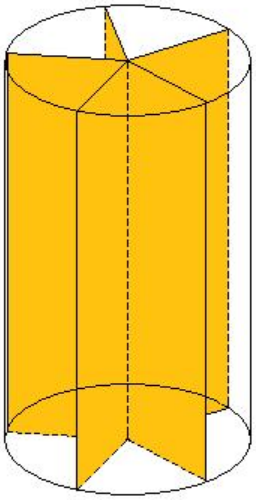

Figure 2.4: The generic arrangement of twin boundaries in a five fold cyclic twinned wire

structure adds to the yield strength of the wires [6]. The work took five fold twinned wires and deformed them to find the extent of the elastic and plastic regions. In order to compare the results to single crystal morphologies, some of the nanowires were annealed to induce recrystallisation. The increased yield strength is due to the to the grain boundaries running along the length of the nanowires. The highly controlled crystal orientations intersect the principle slip directions to harden the structure.

I would expect to see a similar increase in the mechanical properties of boron rich nanowires that are cyclically twinned further augmenting any size effects.

2.4.1 The unit cell of boron carbide.

My work is based on a method that produces boron carbide nanowires. The unit cell of boron carbide is required for simulation of selected area diffraction patterns. The dimensions and atomic positions were taken from work done by Yakel in 1975 [32]. The unit cell has a hexagonal basis with $a = b = 5.6720$ $\mathring{A}$ and $c = 12.1428$ Å. The atomic positions were given as B(1)(-0.164, 0.164, 0.359), B(2)(-0.106, 0.106, 0.133), B(3)(0.000, 0.000, 0.500) and C(0.000, 0.000, 0.383). However, previous work [33] [29] has been done using a rhombohedral basis. The unit cell was converted to a rhombohedral basis. In its rhombohedral form, the unit cell has the following parameters $a = b = c = 5.2065$ $\mathring{A}$ with $\alpha = \beta = \gamma = 65.01$. B(1)(0.195, 0.687, 0.195), B(2)(0.007, 0.325, 0.007), B(3)(0.500, 0.500, 0.500) and C (0.383, 0.383, 0.383). This structure can now be used to analyse the Diffraction patterns, and is directly comparable with the work done previously by others because we have the same basis.

Chapter 3

Experimental methods

> In physics, you don't have to go around making trouble for yourself - nature does it for you.
>
> Frank Wilczek

3.1 Microscopes and Techniques.

During the course of my work many different microscopes were used to analyse various aspects of the nanostructures produces. This chapter describes the equipment used, and details the underlying principles that need to be known in order to extract meaningful information from the results obtained.

3.2 Scanning Electron Microscope.

A Scanning Electron Microscope (SEM) works by using electromagnetic lenses to focus an electron beam into a probe [34]. This probe is then scanned in a raster pattern across the sample. As the electrons travel through the sample they collide inelastically and generate secondary electrons. The secondary electrons can then escape the surface of the material, and be collected by the detector using a bias voltage to attract them. The intensity of emission is measured at every point by collecting the emitted secondary electrons. The intensity recorded at each point is used to form an image by representing each collection point as a pixel. Because more electrons can escape from the edges of samples, i.e. there is a shorter distance to travel before they escape into the vacuum, there is a difference in contrast and this can be used to form an im-

age of surface topography. Due to the vast amount of incoming electrons it is possible for charge to build up if the sample is not sufficiently conducting. The build up of charge on a sample is undesirable as it makes it hard to image the sample at high resolution and the contrast continuously changes.

The SEM is useful for looking at bulk material, it is quite surface sensitive but does permeate into the sample to some extent. The depth of penetration can be changed by varying the acceleration voltage. Different accelerating voltages can be used for different purposes.

3.3 Transmission Electron Microscope.

The Transmission Electron Microscope (TEM) is very useful for the analysis of nanomaterials. It is very versatile and can give a lot of information about the sample. In the TEM the sample is illuminated by a parallel incident beam [35]. The rays travelling through the sample are caused to scatter by interactions between the electrons and the atoms in the sample. These rays are collected by the objective lens and directed into a focal plane and an image plane. Information can be obtained from both the focal and the image planes. In the focal plane the information appears as a diffraction pattern which contains information about the crystal structure and the lattice spacing. In the image plane an image of the sample is displayed. The Diffraction pattern is a Fourier transform of the real space image and is a very powerful tool in the analysis of nanomaterials. It allows for the determination of the structure and can confirm the elemental composition of a sample.

Electrons interacting with the sample are scattered by elastic and inelastic collisions. This scattering crates many imaging conditions that can be used to analyse a sample in the TEM. Because the beam of electrons needs to be transmitted, the sample must be sufficiently thin to allow them to pass through. The thickness of the sample should be less than 100nm to be electron transparent and ideally be less than 30 -50 nm.

3.3.1 Image formation in the Transmission Electron microscope.

The incident beam is a plane wave function. When the incident wave interacts with the sample a scattering phenomenon occurs and many wave functions arise. When the diffracted wave passes through the objective lens the wave function can be directed either into the Focal plane and an image plane as shown in figure 3.1. In the focal plane of the lens we get information in the

form of a Fourier transform and in the image plane the information is in the form of an inverse Fourier transform.

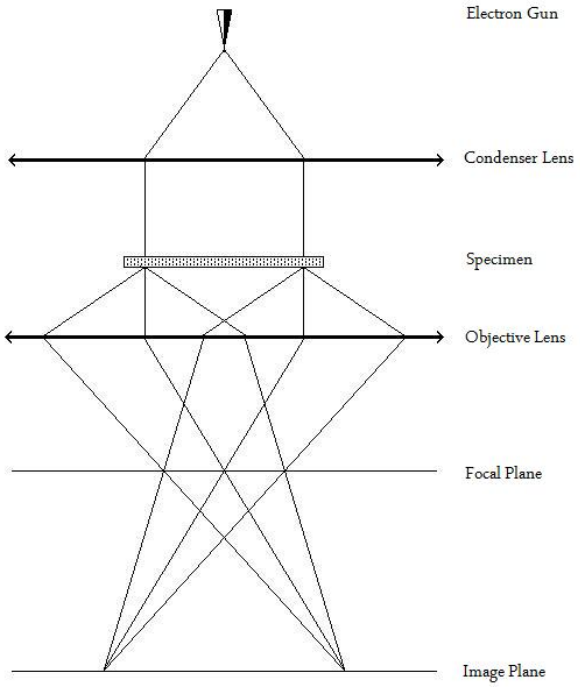

Figure 3.1: The focal and image plains of a TEM

3.3.2 Electron scattering

As the electron beam passes through a crystalline sample the electrons are scattered by the many atoms in the structure. This scattering is described by Bragg's law as shown in figure 3.2 and described by the equation:

$$n\lambda = 2d\ sin(\theta_n) \tag{3.1}$$

Where n is an integer λ is the wavelength of the incoming wave d is the distance between two crystal planes and θ_n is the scattering angle.

This equation can be used to calculate the Bragg angles. At the Bragg angles the intensity of the scattered beam is at its maximum. The resulting diffraction pattern indicates that is due to the inelastically scattered electrons.

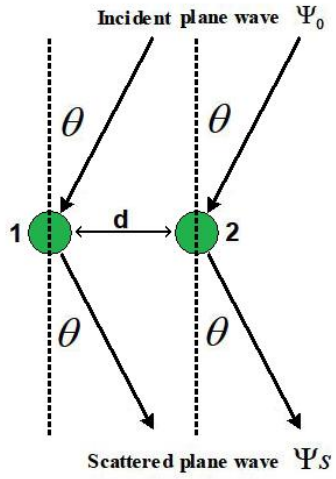

Figure 3.2: Bragg scattering from a crystal lattice. As described by equation 3.1

3.3.3 The origin of contrast.

After the electron beam has passed through the sample, the wave functions vary by angle. The different wave functions hold information about the interaction between the sample and the electrons beam. Contrast is the difference between the intensity of the transmitted beams from different areas of the sample and can be expressed as

$$C = \frac{I_2 - I_1}{I_1} = \frac{\Delta I}{I_1} \tag{3.2}$$

Where C is the contrast and I is the luminance. The objective aperture which is located in the focal plane of the objective lens can be used to select the direct maximum or one of the diffracted maximum to form the image. The direct maximum gives a bright field image and a diffracted maxima gives a dark field image.

3.3.4 Types of imaging.

Contrast can be positive or negative in transmission microscopy. A positive contrast is known as a bright field Image and negative contrast is known as a dark field image. Ray diagrams of the microscope arrangements for each different technique is shown in figure 3.3

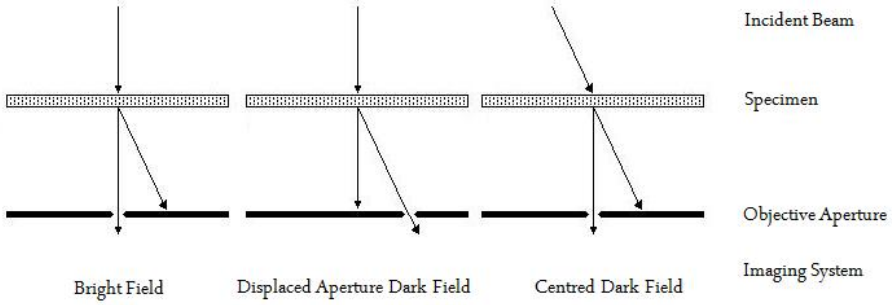

Figure 3.3: The difference between dark field and bright field imaging in a TEM. Forming images relies on diffraction contrast.

3.3.4.1 Bright Field Imaging.

A Bright Field image is produced using the direct beam once the wave has scattered through the sample [35]. The direct beam is the central bright spot in a diffraction pattern. This is the most basic imaging performed in the microscope and is usually the starting point for any analysis. A bright field image appears like a photograph. That is the object removes some of the beams travelling through it to leave a variation in contrast.

3.3.4.2 Dark Field Imaging.

A Dark Field image is formed from a beam that has been scattered by a crystalline sample [35]. These diffracted beams appear as the scattered spots in a diffraction pattern. Dark field images can be obtained in two ways, displaced aperture dark field where the incident beam is normal to the specimen and centred dark field where the incident beam is tilted to the sample. The image is an inverse of a bright field image, that is the object appears bright on a dark background. This can be an useful tool because only the parts of the sample able to scatter to that position will be displayed.

3.3.5 Contrast in the TEM.

Now that we understand what contrast is we shall examine the techniques that can be used in microscopy in order to create contrast and look at what kind of sample each technique is useful for analysing.

3.3.5.1 Mass-Thickness Contrast.

Mass thickness contrast arises from the incoherent elastic scattering of electrons [35]. Thicker areas scatter more electrons than thinner areas. But also in a sample of uniform thickness regions containing atoms with a higher atomic mass will scatter more than regions that contain atoms with a lower atomic mass. The thicker or higher Z areas appear darker in bright field images. The intensity can be described by Beer's law

$$I_{x,y} = I_0 \exp\left(-\left(\frac{\mu}{\rho}\right)\rho t\right) \tag{3.3}$$

Where $\frac{\mu}{\rho}$ is the mass absorption coefficient ρ is the density and t is the thickness. The scattering is dependent on the atomic mass (Z) and thickness variations in the sample. For this reason images taken by this method are mostly qualitatively interpreted. This technique is useful for the study of non-crystalline materials.

3.3.5.2 Diffraction Contrast and the Two Beam Condition.

Diffraction contrast arises from different parts of a sample being in different crystallographic orientations. Parts of the sample scattering more of the electron beam appear darker in bright field imaging. Diffraction contrast is described by Bragg's law, and is dependent on the orientation of crystal planes with respect to the beam of electrons [35].

The two beam condition relies on diffraction contrast. For the two beam condition the sample must be tilted so that only one of the diffracted beams is strong. Several different two beam conditions can be obtained from near a zone axis diffraction pattern by slightly tilting the specimen. Dark field images can be obtained from the strong diffracted beams. The dark field image will vary with the different two beam conditions. By using the two beam condition we can obtain good contrast in our images and also makes interpreting the image much simpler. This technique is useful for examining strain in a crystal lattice.

3.3.5.3 Phase Contrast Imaging.

Unlike other imaging techniques phase contrast imaging uses the phase differences between diffracted electron waves [35]. This technique is used for the imaging of crystalline materials. Both transmitted and refracted beams are

gathered, the contrast is a result of the phase difference between the diffracted and transmitted beams.

Whilst most imaging techniques use variation in the amplitude modulation to see the object, phase contrast imaging uses changes in the phase. The variations in the phase are induced by variations in the object. We cannot detect phase variations, so we have to transform the phase modulation into an amplitude modulation. This is done by the interference of the transmitted and refracted beams. The difference in phase between the two causes interference, which in turn changes the amplitude of the wave.

In simple terms: If we have an incoming wave

$$E_i(x,t)|_{x=0} = \mathbf{E_0} sin(\omega t) \tag{3.4}$$

The object will induce a phase variation

$$E_{PM}(\mathbf{r},t)|_{x=0} = \mathbf{E_0} sin[\omega t + \varphi(y,z)] \tag{3.5}$$

Using a trigonometric identity we can write this as

$$E_{PM}(y,z,t) = \mathbf{E_0} sin(\omega t) cos(\varphi) + \mathbf{E_0} cos(\omega t) sin(\varphi) \tag{3.6}$$

Usig only small values of φ we get

$$E_{PM}(y,z,t) = \mathbf{E_0} sin(\omega t) + \mathbf{E_0} \varphi(y,z) cos(\omega t) \tag{3.7}$$

The first term is independent of the object, so if we change the relative phase by $\pi/2$, we get

$$E_{PM}(y,z,t) = \mathbf{E_0} \big[1 + \varphi(y,z)\big] sin(\omega t) \tag{3.8}$$

This is an amplitude modulated wave. The phase variations in the electron beam are not recordable, so we use this technique to transform the imaginary phase information into a component of the amplitude of the wave function.

This is a real number and can easily be recorded.

3.4 Scanning Transmission Electron Microscope.

The Scanning Transmission Electron Microscope (STEM) is similar to the SEM because it forms the electron beam into a probe at the sample and scans the surface in a raster pattern [35]. But unlike the SEM the beam is transmitted. So the sample must be sufficiently thin (as in the TEM). For STEM the elastically scattered beams of electrons are used to form the image, they are collected by Annular Dark Field (ADF) Detectors and High Angle Annular Dark Field (HAADF) Detectors. HAADF images are highly dependent on the atomic number (Z) of the sample because more electrons are elastically scattered by atoms with a higher atomic number. Heavier elements appear brighter that lighter elements in HAADF images. The inelastically scattered electrons can be used for EELS.

3.5 Chemical Analysis.

In many instances, when looking at materials in a microscope it is desirable to know what elements are present in the sample and in what concentration. In order to do this several techniques have been developed that permit us to perform chemical analysis in the microscopes. Here we deal with two that were used during the research.

3.5.1 Electron Energy Loss Spectroscopy.

Electron Energy Loss Spectroscopy (EELS) uses the transmitted beam from the STEM i.e. the beam that is not scattered to high angles due to scattering inelastically. As the beam is transmitted through the sample its energy is changed by interactions with the atoms present in the sample. Because we know the energy of the beam before the sample, any changes are caused by the sample itself [36]. This allows us to identify which elements are present in the sample by looking at the characteristic energy losses. An EELS spectrum contains three distinct regions. A Zero loss peak, low loss region and high loss region. Each region provides different information about the sample. These different regions are shown in figure 3.4

1. The zero loss peak is formed by electrons that have simply passed through

the sample without interacting with it and elastically forwards scattered electrons.

2. The low loss region is formed by the interaction of the beam with the outer electrons of the atoms.

3. The high loss region is due to electrons interacting with the tightly bound inner electrons. This region carries the element specific information and information about the bonding.

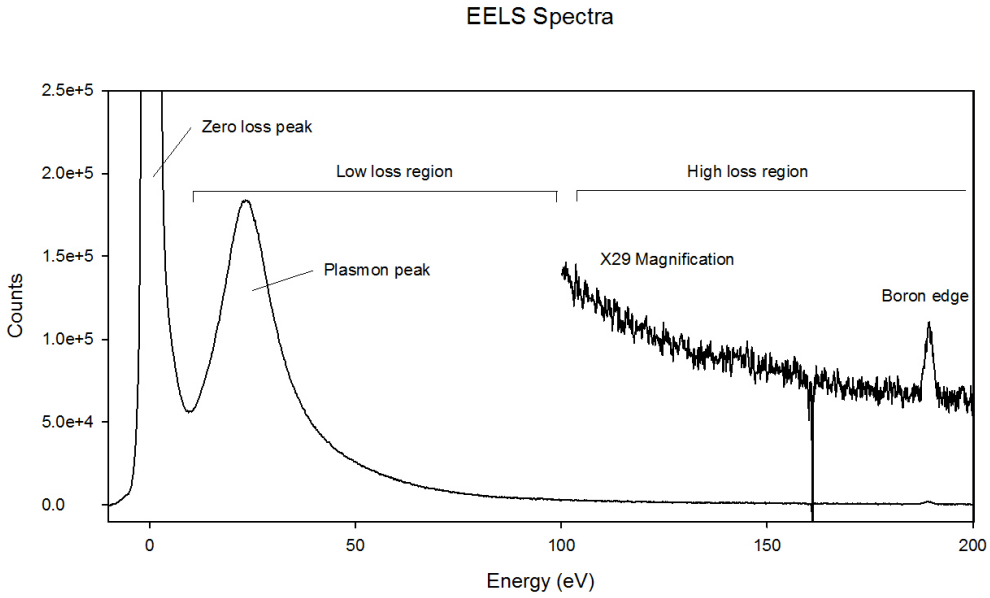

Figure 3.4: A typical EELS spectrum from a boron carbide nanowire.

When a spectrum is obtained it has a background and a set of edges. The background arises from multiple inelastic electron scattering events or the extension of previous absorption peaks. The background decays rapidly as a power law. To get an elemental ratio the background must be subtracted to leave the edges isolated.

EELS can also be used to measure the thickness of the sample by comparison of the zero loss intensity to the spectrum intensity.

3.5.2 Energy Dispersive X-ray Analysis.

Energy Dispersive X-ray (EDX) analysis is a technique that uses the characteristic emission of x-rays from atoms as the electrons drop into lower orbitals [36]. As high energy electrons pass through the sample, they collide with the electrons orbiting atoms in the sample. If an electron manages to displace an inner shell electron from an atom an electron from a higher electron orbit will

drop into the vacant position emitting an x-ray as it does so. These x-rays are constantly emitted, and can be detected for use in chemical analysis. Each energy gap is different and therefore will produce an x-ray with an unique energy. The energy is measured by the detector and compared to known values of element specific x-rays. In this way elements present in a specimen can be identified. Also the abundance of the element can be found by tallying the counts at these specific energies. If EDX is used in conjunction with a scanning probe then the elements at a specific location can be identified or regions of the same element mapped. However the accuracy of EDX is limited by the skin depth of the electrons as X-rays can be produced anywhere within the sample that the electrons can penetrate to. Also the detector can only capture a small amount of x-rays due to the uniform angular distribution of emission and the fact that x-rays cannot be focused by lenses. An example of an EDX spectrum is shown in figure 3.5

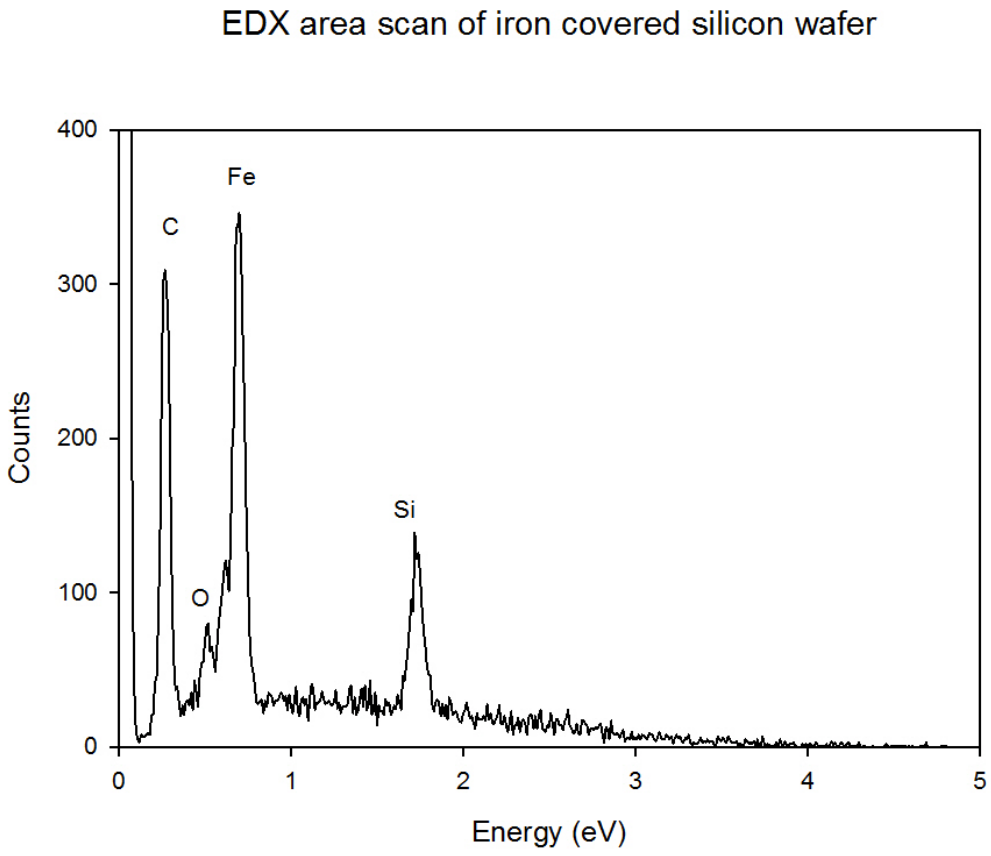

Figure 3.5: A typical EDX spectrum of an iron coater silicon wafer.

As a general rule of operation the accelerating voltage of the electron gun should be at least twice the value of the characteristic x-ray you wish to observe. This is to make sure that the excitation of the electron can take place.

Chapter 4

Results

> Science is always wrong. It never solves a problem without creating ten more.
>
> George Bernard Shaw

4.1 Preliminary work

This chapter documents the procedure of designing and implementing an experiment to grow boron rich nanostructures. The ultimate aim of doing so is to study the growth and confirm that it is vapour based and to examine the parameters that effect the growth in order to lead to optimisation.

Samples were initially produced using a method based on the work done by jiang *et al* [28] to produce nanowires on powder pellets. Powders of B, BaO and Fe_3O_4 were mixed in an agate pestle and mortar until they formed an uniform brown powder (approximately 10 minutes). Drops of glycerine from a pipette were added one at a time and mixed into the powder until the powder was uniform again. Three drops of glycerine were used with $0.411 \pm 0.01g$ Fe_3O_4, $0.301 \pm 0.01g$ B and $0.288 \pm 0.01g$ BaO.

In order to fire the sample in the furnace the powder mixture was pressed in a die to form a disk 20 mm in diameter and approximately 1mm thick. A Clarke Workshop Bench Press (10 Ton) was used for this purpose. Approximately 6 tons of weight was used to form the pellet in the industrial workshop bench press. Six tons refers to the maximum pressure in the hydraulic ram when the die was underneath it.

All samples used in this work were produced using this procedure and ingredients.

To form the nanostructures the powder needs to be fired. To fire the powder an Ellite Thermal Systems Limited TSH16/75/450 tube furnace was used with integrated Eurotherm 2416 PID and 2116 Overtemperature controllers. The gas flow for the tube furnace was controlled by an MKS Mass Flow Controller (MFC) Type 1179A with a maximum flow of 200 sccm and calibrated to argon. The MFC was controlled by a MKS PR 4000 control box. The exhaust gas was passed through a sealed glass bottle half filled with water in order to remove particulates and prevent gas travelling up the exhaust. The set up of the furnace is shown in figure 4.1. Further details of furnace operation and procedures are included in Appendix A, along with Standard Operation Procedure (SOP) and health and safety forms.

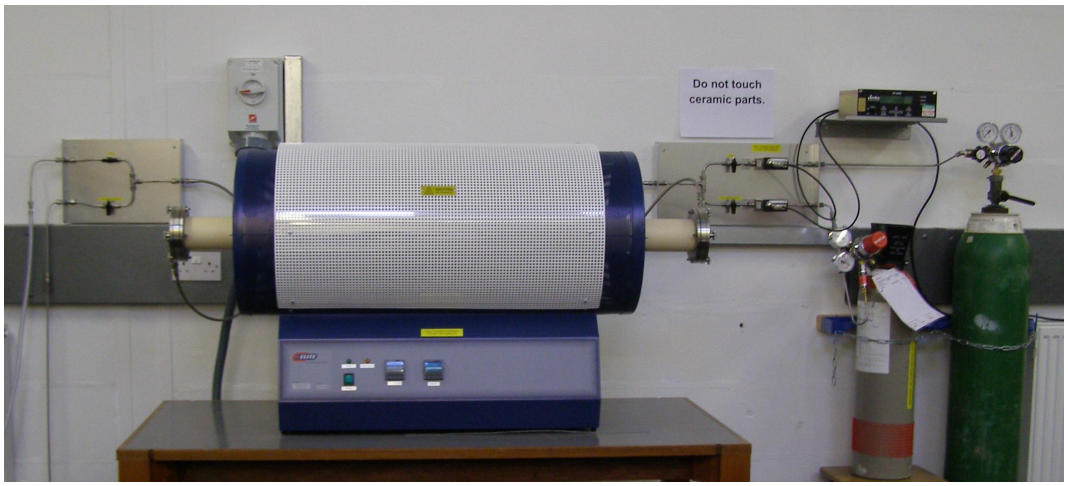

Figure 4.1: The furnace and gas flow system

The powder was put in an alumina boat and placed in the centre of the tube furnace. The system was flushed with argon gas at 200 sccm to flush the system, before being heated at 7°C per minute from room temperature to 200°C. Whilst the temperature was being raised the flow of argon gas was maintained at 200 sccm. Once the temperature reached 200°C the gas flow was reduced to 60 sccm and the temperature was raised at six degrees per minute to the maximum temperature of 1300°C. The furnace was held at this maximum temperature for sixty minutes. Once the program had finished the furnace was allowed to cool by natural convection to room temperature. The argon was kept flowing until the furnace was completely cooled.

Examination of the sample shows that nanostructures were successfully grown. The structures were observed in SEM and the powder dispersed in isopropanol to make TEM samples.

Figure 4.2 shows some of the nanostructures observed on the samples and are very similar to the nanostructures described in the literature [27][28], As mentioned in much of the literature there is a droplet structure at the end

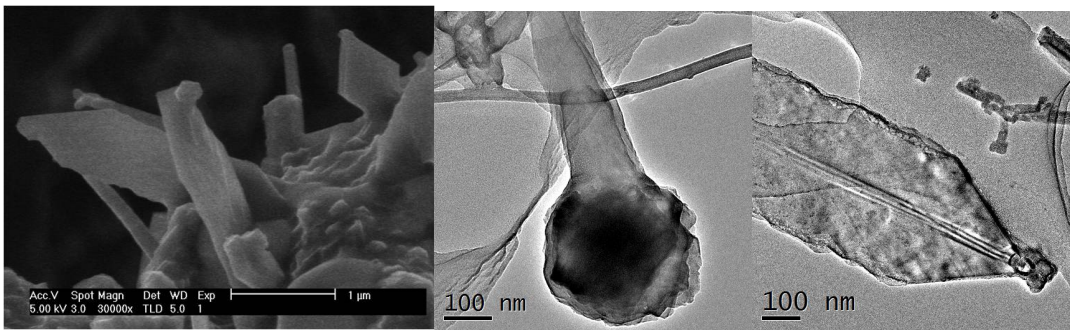

(a) (b) (c)

Figure 4.2: A selection of nanostructures from the powder sample. (a) SEM image showing platelets and wires. TEM images of (b) nanowire with droplet structure at tip and (c) Platelet.

of many of the nanostructures. The dark contrast indicates the possibility of these droplet structures containing iron. These may have a catalytic role in the growth of the nanowires and are an indication that the nanomaterials may be grown via a VLS route as suggested by [27] and [29].

In producing these samples we were able to investigate the role of barium oxide in the samples. This was done to give us a greater understanding of how the concentration of barium would affect the size of the nanostructures grown. It should be noted that the nanostructures examined in this part of the work are the platelets, such as the one shown in figure 4.2 c)

Several mixes of powder was prepared with a varying concentration of barium oxide. The barium oxide was varied from 1.5% to 10.8% by weight. After the pellets were fired they were examined by Scanning Electron Microscope and Transmission Electron Microscope.

The graph in figure 4.3 shows that there is an increasing trend in the width of the platelets with an increase in the concentration of barium. The barium could be promoting growth by helping to produce a greater amount of the boron rich gas needed for the VLS based growth.

4.2 Proving VLS growth.

The aim of this work is to determine how the unique fivefold structure is grown. Work such as Cao *et al* [27] suggests that the presence of a catalytic droplet means that the growth is likely to be grown by a VLS method. I will now continue to attempt to prove that this is the case. According to the theory of VLS growth [11], the growth of the nanomaterials can occur at any site where the catalytic particle is present. This means that the nanomateri-

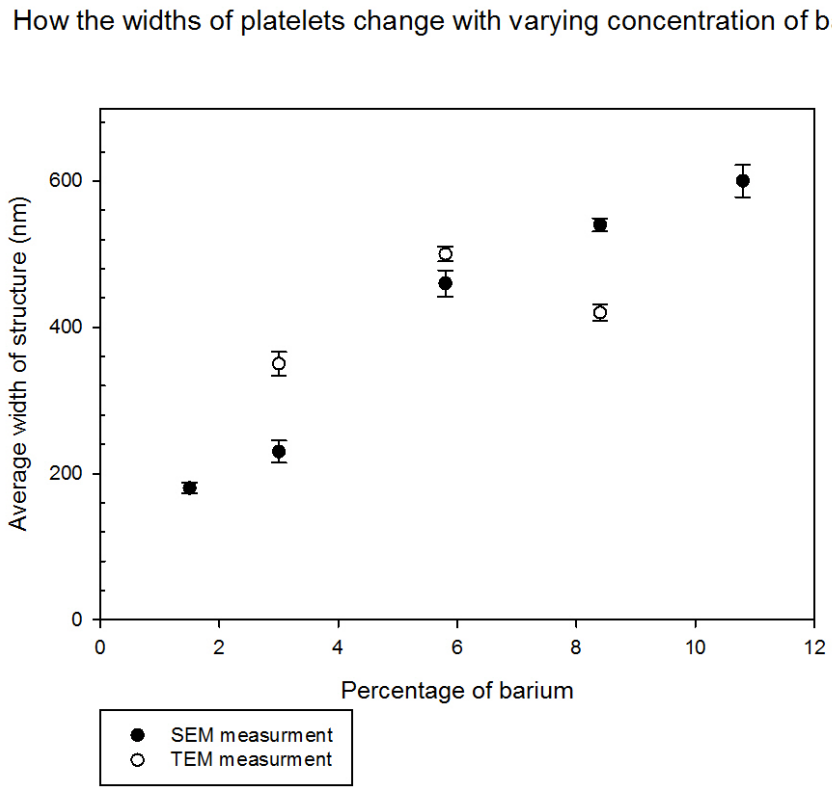

Figure 4.3: Variation of average diameter distribution with respect to barium concentration.

als should be able to grow on a remote site. This can be used to prove that VLS growth is present by having the catalyst located on a remote site. If nanostructures grow then they are grown by a form of the VLS method. It was decided to use a Silicon wafer was the substrate.

4.2.1 Designing an experiment to isolate VLS growth.

The evidence for VLS growth is the presence of droplets at the tips of the nanowires that are present in the previous work done on boron rich nanostructures grown by a similar methods such as [27]. Also the eutectic point between the components points towards the possibility of VLS growth at temperatures exceeding 1100°C.

In order to test this proposal it was decided to design an experiment that would isolate the VLS growth. Because VLS growth uses a vapour phase, it is possible to have the gas produced in the pellet travel in the flow of argon to a remote site where the liquid metal catalyst is present on a substrate.

Wafers of silicon (110) were sputtered with iron in a High Target Utilisation Sputtering (HiTUS) system. The thickness of the iron layer was arbitrarily set to 30 nm. The silicon wafer was cut into pieces measuring approximately

20mm by 5mm. After the film was grown, it was exposed to the atmosphere, so it is safe to assume that the iron is oxidised.

The iron coated silicon wafer was placed approximately 15mm downstream along with a plain piece of silicon to act as a control in the flow of argon from the powder pellet used to create the boron rich gas. The furnace was heated using the same procedure as described in section 4.1. The specimen was removed from the furnace once it had cooled to room temperature. Using a light microscope with a x1000 magnification to examine the surface of the wafer figure 4.4 was obtained. Structures are clearly visible on the surface.

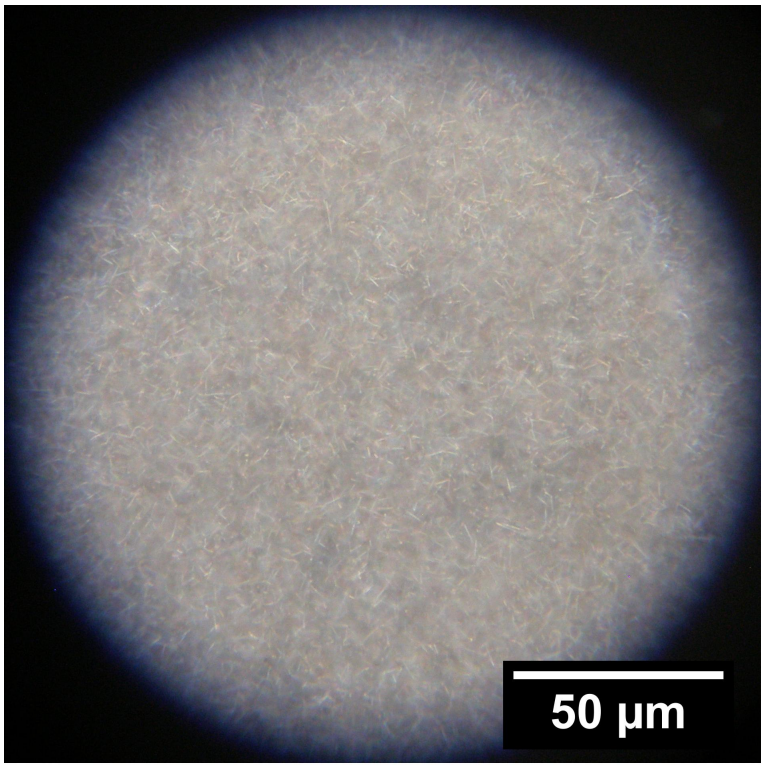

Figure 4.4: A light microscope image of the surface of the wafer taken at x1000 magnification.

4.2.2 SEM examination.

A JEOL SEM (JSM 7000F) was used to study the morphology of the nanostructures grown. This was done by obtaining secondary electron images of the surface of the silicon wafer. The structures were examined specifically for the characteristic details of the five fold multiple twinned nanowires.

The light microscope image figure 4.4 and the electron micrograph figure 4.5 a) clearly show a large coverage of wires on the substrate. Figure 4.5 a) is over an area roughly 100 by 150 μm, (roughly 15mm square). This shows that this method of growing nanostructures gives an uniform density of nanostructures

over a large area. Also visible are the characteristics of the multiple twinned wires: a difference in contrast is clearly visible at the centre of some of the wires indicating a variation in topography resulting from the star shape cross section. A good indication that the growth is due to a VLS method is the presence of the droplets on the tips of the nanowires. In addition to those nanowires displaying these characteristic structures there are other structures that could be single crystal. Also observed are the broad flat nano platelets that are also found in the powder samples.

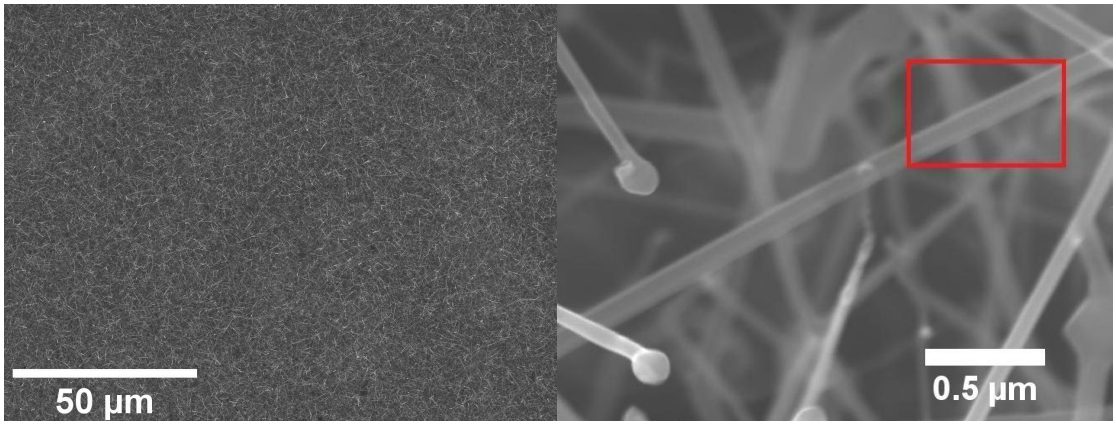

(a) (b)

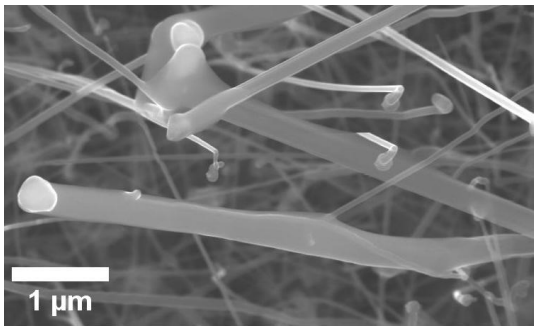

(c)

Figure 4.5: a) Shows an uniform covering of nanowires. b) and c) are higher magnification images showing droplet structures at the end of the wires. Also visible in b) is a nanowire showing the characteristic variation in cross section, indicated by rectangle.

These images also clearly show the presence of the droplet structure at the end of the wires. This is indicative of VLS growth, and is a good indication that we have managed to isolate the VLS growth component responsible for the formation of the five fold twinned nanowires. In figure 4.5 c) a variation of morphology can clearly be seen in the region of the wire indicated by the box. This is due to the multiple twinning of the particle and is a clear indication that we have the presence of the multiple twinned nanowires that are also found in the powder samples. These re-entrant edges are discussed in great detail by

Fu [29].

Because the nano structures are grown without any clear preferred direction of growth, it is difficult to find the base of the nanowires. This makes the study of the base of the nanowires difficult. It also inhibits the measurement of the lengths of the nanowires. However it is possible to move our observations to the edge of the silicon wafer and look at structures protruding over the edge or those grown on the sides of the silicon wafer.

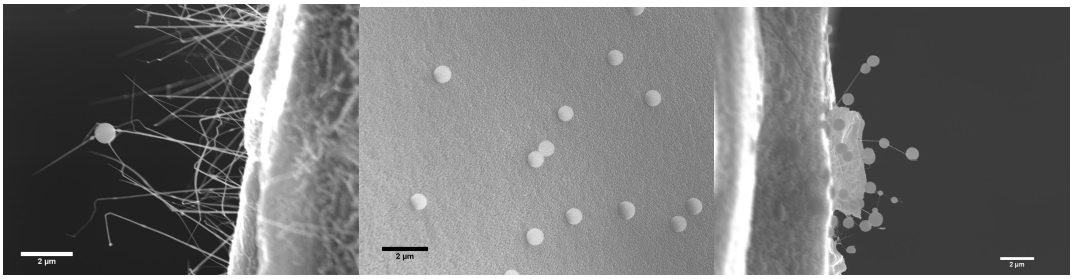

(a) (b) (c)

Figure 4.6: These SEM images show nanowires at the edge of the silicon wafer. a) nanowires including one with a large droplet structure. b)droplet structures on the silicon substrate c) nanowires with an extensive covering of large droplet structures.

In figure 4.6 a) we can see that the length of the wires is easier to determine. The base of the wire is still not visible but it is possible to estimate where it is without incurring an overly large error in length calculation. In figure 4.6 b) we can see droplets on the side wall of the silicon wafer, we can also see similar droplets along the length of the nanowires in figure 4.6 c) however these are much larger than droplets observed on other parts of the sample, this could be due to a larger volume of boron rich gas passing over these lower density nanowires in comparison to the nanowires at the centre of the silicon wafer.

From observations we can say that the length of the nanowires grown is roughly 10 μm microns. In principle it should be possible to vary the length of the nanowires grown, by varying the length of time that the boron rich gas is passing over the substrate and catalyst. However accurate control of how long the boron rich gas is passing over the catalyst is not very controllable in the current system. Improvements to the method used will be discussed later on in section 5.2.

4.2.3 TEM analysis.

The microscope used to do this analysis is a JEOL 2011. In order to determine the types of nanowires produced TEM samples were prepared by using a clean

scalpel blade to scrape the surface of the silicon wafer over a vial. The vial was then part filled with isopropanol and then dispersed in an ultrasonic bath for a few minutes. The isopropanol was then dripped onto holey carbon film supports mounted on copper TEM grids. When the sample is loaded into the TEM the individual nanowires can be examined. In the microscope bright field images were obtained.

Using the TEM micrograph obtained during the course of the work, 36 wires were recorded as examined with 25 of the nanowires being multiply twinned, 9 single crystal and 2 were amorphous. If this is a representative sample of the nanowires produced then $\sim 70\%$ of the nanowires produced are multiply twinned. However there is the possibility that twinned nanowires appear as single crystal due to only one segment being in diffraction condition, and for single crystal nanowires to have defects present that may cause the diffraction pattern to look like a twinned pattern.

4.2.4 Amorphous nanowires.

Some of the wires observed were amorphous. These wires tend to have a rough surface and curve slightly.

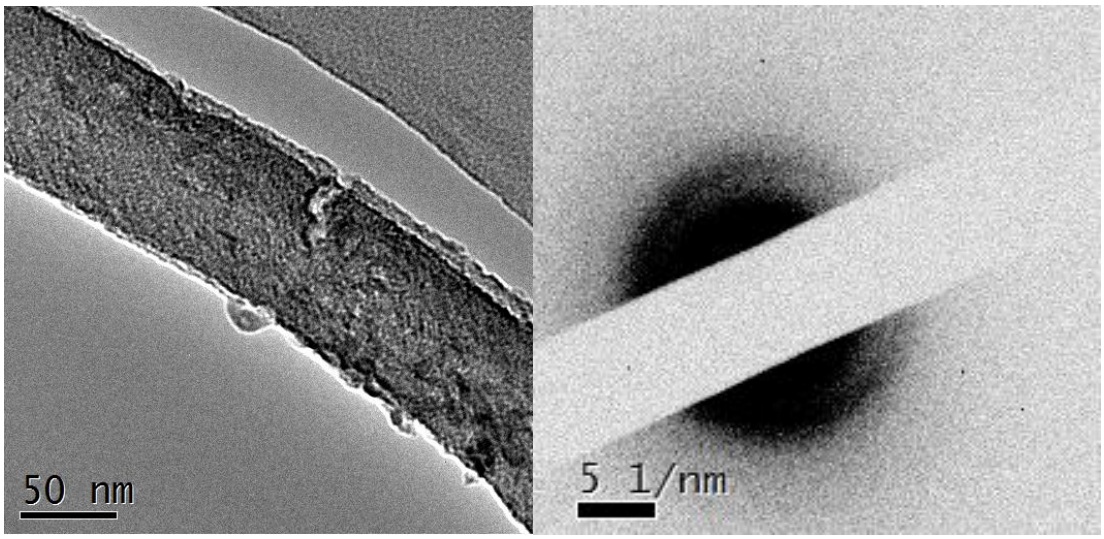

(a) (b)

Figure 4.7: Bright field image of nanowire a) associated diffraction pattern b) of an amorphous nanowire.

Figure 4.7 a) is a bright field image of one such amorphous nanowire. We can see it has a very rough surface and also there is a slight curve visible in the wire. The wire is confirmed as an amorphous nanowire by looking at the associated diffraction pattern figure 4.7 b).

The wire could be a boron rich amorphous nanowire or it could be a silicon wire. The silicon wire would form from the substrate. This is made possible due to the surface modification of the wafer at the experimental temperature of 1300°C. Looking at the images in figure 4.8, the modification caused to the surface of the silicon wafer without iron can be clearly seen. The wafer was cleaved and the piece rotated so that the cloven facet faced upwards. The resulting SEM micrograph figure 4.8 b) shows that the destruction of the surface of the wafer extends approximately $20\mu m$ from the surface.

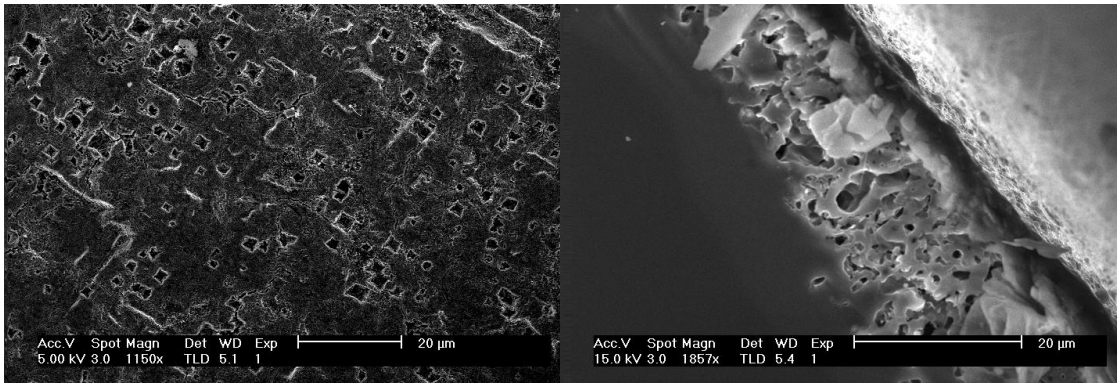

(a) (b)

Figure 4.8: The damage caused to the substrate by the high temperature of the furnace from above a) and in cross section from a cleaved silicon wafer b)

The damage caused to the surface may cause silicon vapour that may be incorporated into the nanomaterials and form amorphous nanowires. Single crystal silicon nanowires may also be formed with the addition of an iron catalyst [37].

4.2.5 Single crystal nanowires.

Some of the nanowires displayed diffraction patterns for single crystal nanowires. To examine the crystal structure, Selected Area Diffraction was used.

4.2.5.1 Electron diffraction analysis of individual nanowires.

In order to confirm the crystal structure of a single crystalline nanowire, several diffraction patterns were obtained from different zone axis. The sample was orientated using a double tilt holder. When a diffraction pattern is on a zone axis the pattern is symmetrical. Three of these patterns were obtained and compared to computer simulations. The simulations were constructed using two pieces of software.

1. CrystalKit - A program to construct a three dimensional model of the unit cell from known basis and atom locations.

2. MacTempas - Mainly used for high resolution image simulation, but in our case used to construct and index the diffraction patterns.

The structure of boron carbide detailed by Yakel [32] was used to create an unit cell with CrystalKit, and the lower order diffraction patterns were calculated using MacTempas. These patterns were indexed and then compared to the diffraction patterns obtained from experiment. The details of the unit cell used are given in the background.

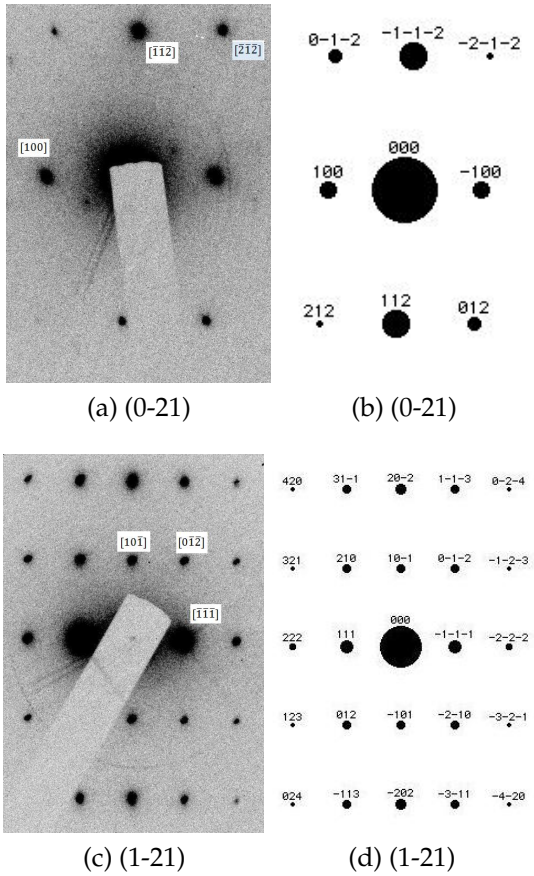

(a) (0-21) (b) (0-21)

(c) (1-21) (d) (1-21)

Figure 4.9: Diffraction patterns of (0-21) and (1-21) orientations from the same nanowire a) and c), and a comparison to simulations b) and c).

The patterns in figure 4.9 are a good match. This confirms that the single crystalline nanowire is likely to be a boron carbide nanowire.

4.2.6 Cyclically twinned nanowires

Figure 4.10 a) shows a nanowire that gives the characteristic diffraction pattern shown in figure 4.10 b) associated with twining. The nanowire is straight and

variations in contrast along the length indicate that some difference in diffraction condition.

Many of the nanowires that were observed displayed the characteristic splitting of the diffraction spots that is a result of the twinned nature of the nanowire.

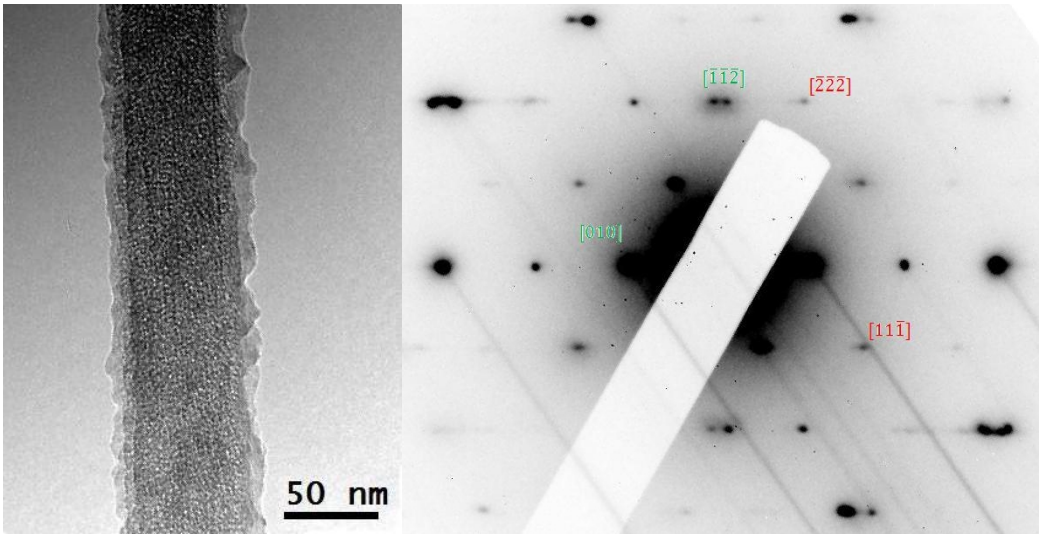

(a) (b)

Figure 4.10: Bright field image a) of nanowire and the associated diffraction pattern b) showing characteristic diffraction pattern due to twinning.

4.2.6.1 Dark field images.

In order to show that the splitting of the diffraction spots is caused by the twinning, dark field images of a wire were obtained. Dark field images are taken by isolating a single diffraction spot from a diffraction pattern using the objective aperture. This condition allows only the parts of the material responsible for producing that particular diffraction spot to be imaged. This is particularly useful when dealing with twinned samples because the cyclically twinned nanowire is made of five crystalline segments each sharing a common crystal plane at the centre each segment has an unique orientation. This means that if we use the objective aperture to isolate a diffraction spot then only the segment of the wire responsible for that diffraction spot will be imaged. By doing this we can confirm that twins are present in the sample.

Dark field images were taken of some nanowires displaying the diffraction pattern that indicates a possibility of multiple twinning.

Figure 4.11 b) shows a comparison of the dark field images obtained from different halves of a split diffraction spot (circled in figure 4.11 a)). It can clearly be seen that each half of the wire is in diffraction condition when each half of

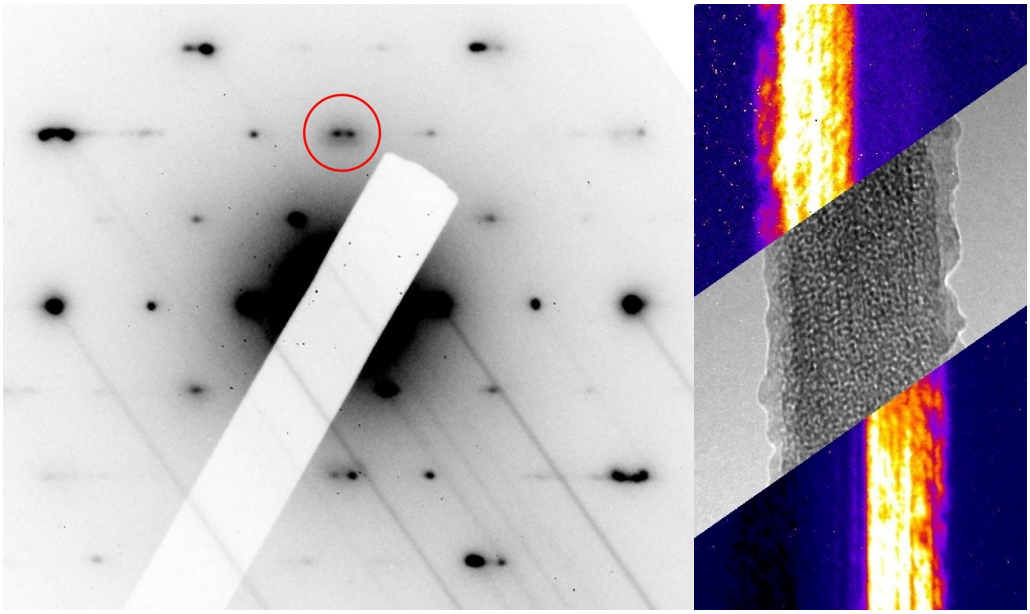

(a) (b)

Figure 4.11: a) Diffraction pattern a) used to obtain dark field images b) from different halves of a split spot (circled), compared with a bright field image.

the diffraction spot is isolated. The images have been coloured to help show the variation in contrast. This allows us to say with certainty that we have a presence of twinned nanowires.

4.2.6.2 Simulation of the twinning diffraction pattern.

The dark field images confirm the presence of a twinning structure, but do not confirm that the wire consists of five twins. In order to show that five fold twinning present, The SAD patterns in figure 4.10 b) was compared to a set of diffraction patterns made from simulations.

The simulated diffraction patterns are constructed from the unit cell described in section 2.4.1. The five fold structure is constructed from the unit cell in varying orientations about a central [001] axis.

In figure 4.12 a) I have been able to isolate four distinct diffraction patterns from figure 4.10 a). There is a possibility that the fifth is not in diffraction condition, or that it overlays on the other patterns. These individual diffraction patterns have been colour coded in figure 4.12 a) in order to show the individual contributions from all the segments. When this simulated pattern is superimposed on the diffraction pattern obtained from experiment, we can see that there is good agreement.

The diffraction patterns are in good agreement with the simulations although

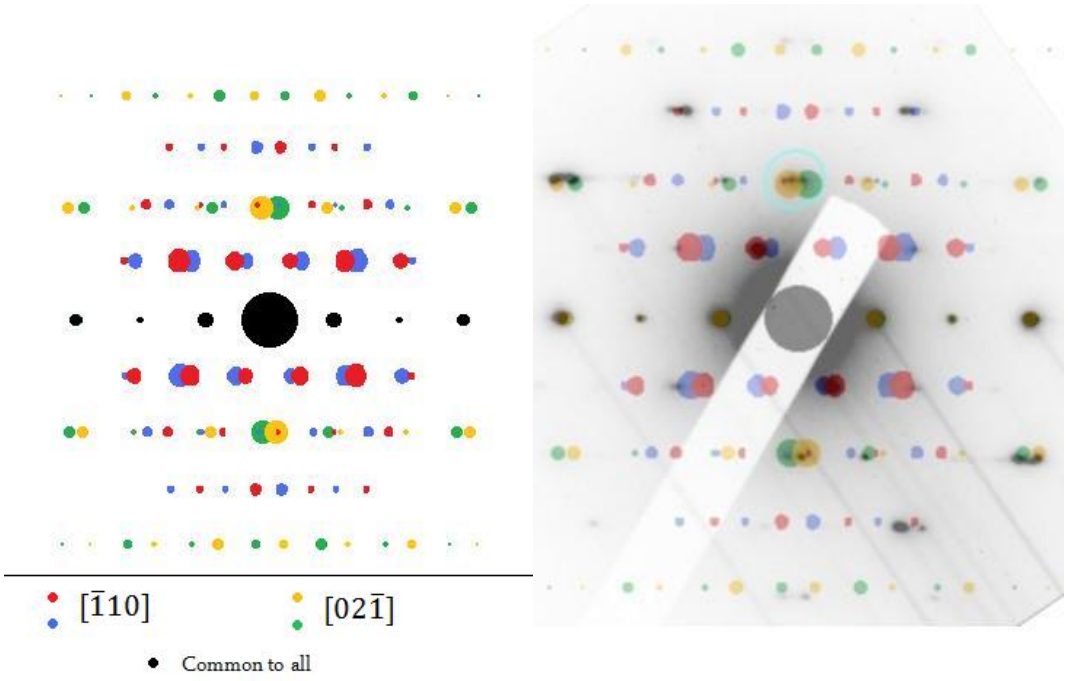

(a) (b)

Figure 4.12: Simulated diffraction patternmade from four different orientations of a boron carbide unit cell a). Simulation overlaid on an experimental result b).

there are some minor discrepancies regarding the intensities, but these could be due to the simple way this pattern was constructed. This tells us that it is highly likely that we have five fold cyclically twinned structures present in the sample grown. This increases the likelihood that we can confirm that these highly unique nanowires are grown via VLS.

4.2.7 Chemical analysis using EELS and EDX

Both EELS and EDX are very powerful tools for performing analysis on the elements that are present in a material. The two techniques use different methods to confirm which elements are present in the sample. We can be certain of the elemental composition of our nanostructures if we are able to obtain results that agree with each other using different elemental composition analysis techniques. To determine the chemical composition of the nanowires an FEI SEM equipped with NORAN system EDX for chemical analysis was used to examine characteristic emission of x-rays from the sample.

When an area of the sample was examined with EDX we can see peaks for boron, carbon and oxygen figure 4.13.

The boron comes from the boron rich gas produced in the pellet, the silicon is

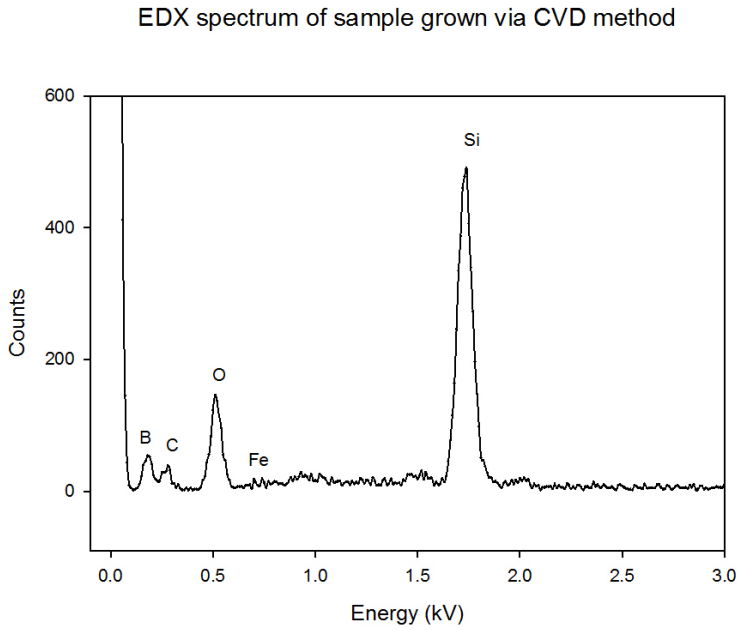

Figure 4.13: EDX spectrum from the surface of the silicon wafer. No peak for iron is seen even though it is expected.

due to the wafer that the structures are grown on, although there is a possibility that silicon nanowires have grown due to the destruction of the surface. The oxygen contribution is likely to come from the silicon oxide layer on the surface of the wafer. The carbon is from the glycerine used to bind the powder when it is pressed. This was also observed by Fu *et al* [29].

A JEOL 2200 FS double aberration corrected microscope operating in STEM mode was used to obtain EELS spectra.

From looking at the EELS spectrum shown in figure 4.14 a) we can see the edges for boron and for carbon, however when we look for the peak for oxygen (532 eV) no peak is visible in figure 4.14 b). This leads us to the conclusion that we have produced boron carbide nanowires and not boron suboxide nanowires.

The background of the signal can be removed by fitting the region just prior to the peak with a power law function. Subtracting this function from all points of the edge leaves only the edge. Once the edges for boron are isolated we can compare the shape of the edge with known edge shapes figure 4.15 c) doing so we can see that there is a good match with see that they are of the same shape as would be expected for a boron carbide material.

The fine structure of the background subtracted edge compares well to the boron carbide edge from the literature [38]. By using the software on the microscope we can quantify the amount of each element present in the sample. This is done by subtracting the background to leave only the signal, the ratios

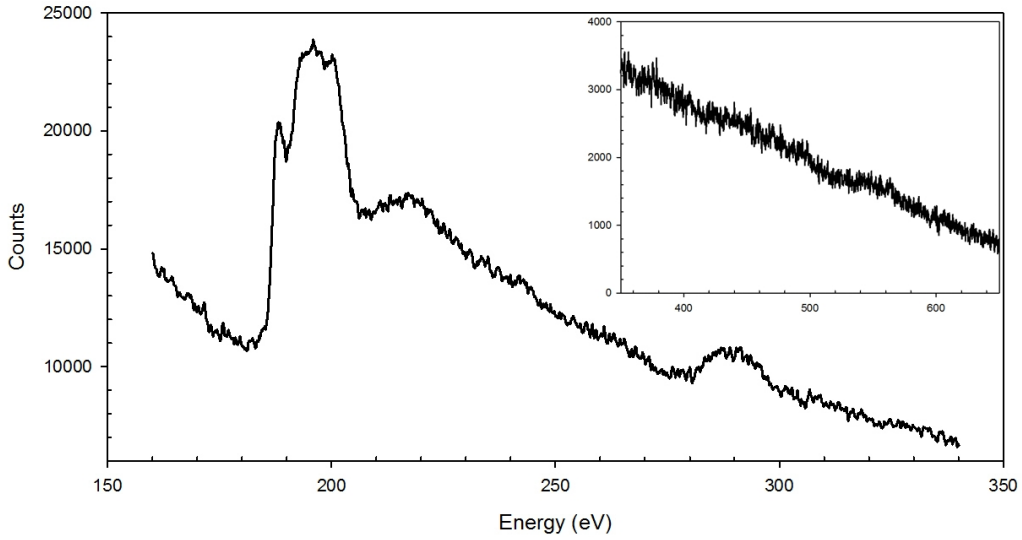

Figure 4.14: Raw EELS spectra showing edges for boron and carbon. Insert shows region surrounding 532 eV where edges for oxygen would be expected.

of the two elements are then compared. The software takes into account the differences between the elements and adjusts accordingly. The results of these calculations are shown in table 4.1.

Carbon	Boron	percentage boron
1	0.83 ± 0.118	45.41
0.39 ± 0.056	1	71.69
0.33 ± 0.046	1	75.43
0.29 ± 0.041	1	77.33
1	0.56 ± 0.080	36.10

Table 4.1: Composition ratios of boron to carbon in the nanowires.

We can see that the ratio of boron to carbon of 3:1 although one ratio does suggest that it is close to 4:1. The build up of carbon on the surface of the wires as scans are performed could be responsible for altering the ratio. A HAADF image pre EELS and post EELS were taken to see if there was any build up of carbon figure 4.16). The scan was performed over the area indicated by the box. The probe was raster scanned over this area to minimize build up of carbon at each point. When the images are compared we can clearly see that there has been a visible build up of carbon (indicated by arrows). This would affect the measurements taken.

The findings of the EELS are consistent with the results from the EDX, We can confirm that we have a presence of boron carbide nanowires. This finding points to the likelihood that the boron carbide nanowires are produced via the VLS path.

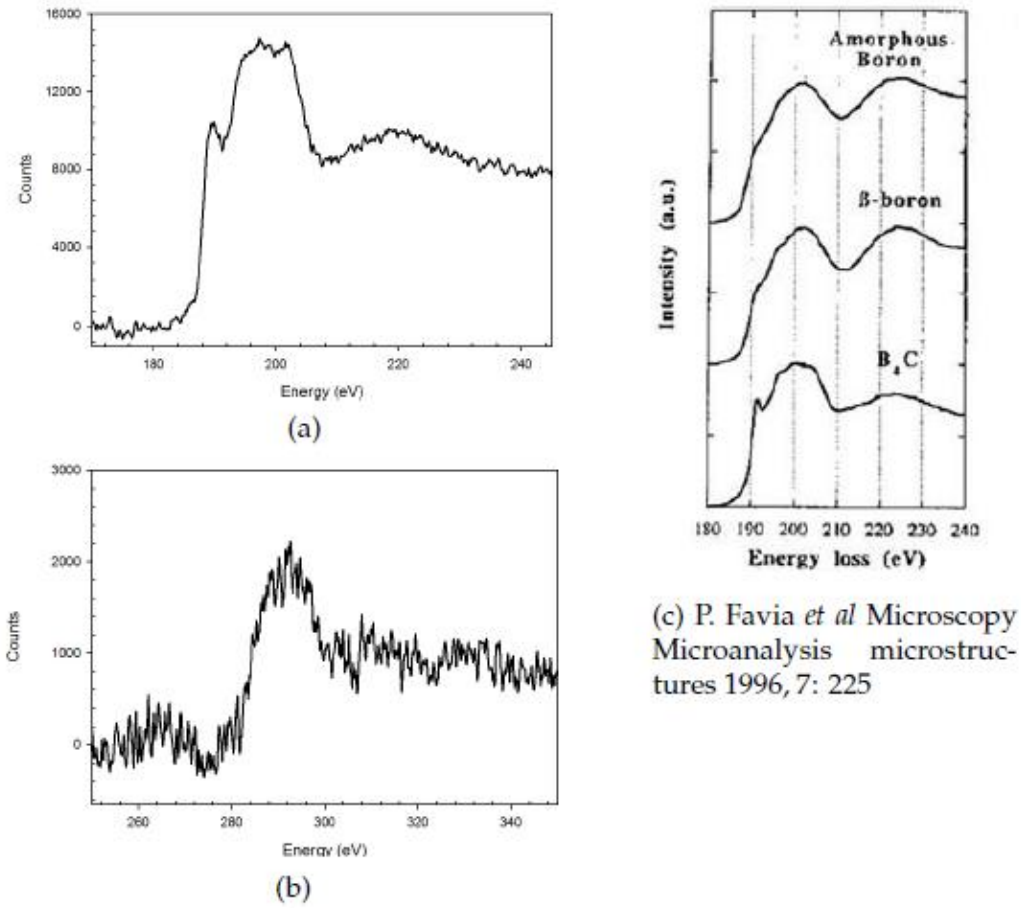

Figure 4.15: Fine structure in the boron edge a) and in carbon edge b). The edges for boron rich materials c).

4.2.8 Summary of Improvements In the method.

When this method of growing nanostructures is compared to the method first used to produce the nanostructures as described in section 4.1, we can see that there are some great differences in the results.

Previously the nanostructures were grown in the powder sample, but with the method discussed in this chapter the nanowires are grown on the flat surface of a silicon wafer. This makes observations of the wires much easier as they are not located on a rough surface.

Comparing images from samples grown at the same time, figure 4.17 a) is from the powder and figure 4.17 b) is from the surface of the silicon wafer. The magnification of the two images is roughly similar, and it can clearly be seen that the density of nanostructures is higher when grown on the silicon wafer. We can also see that the growth covers a larger area when compared to the nanostructures grown on the powder sample.

Growing the nanostructures on the surface of a silicon wafer gives us a high

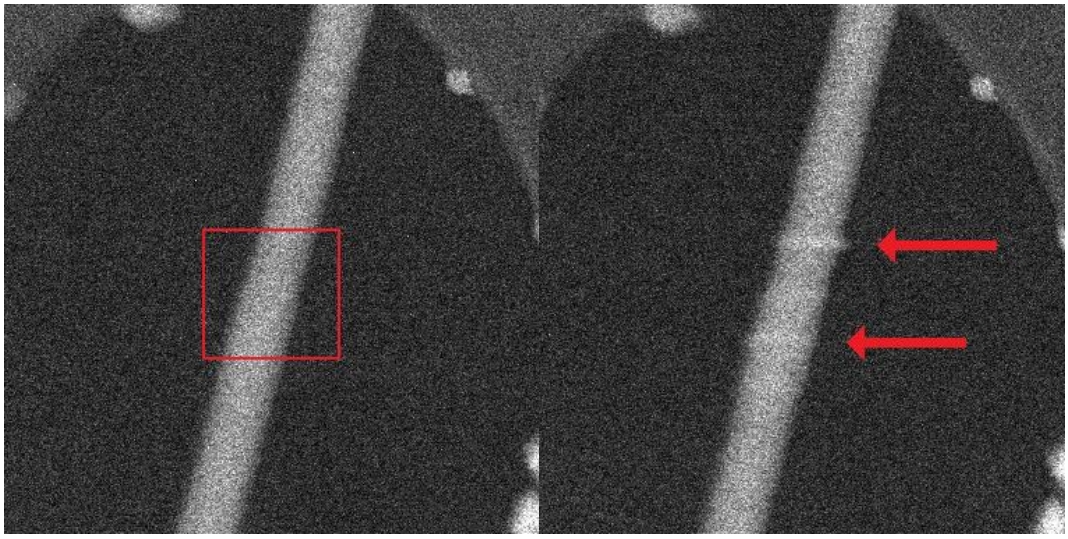

(a) Pree EELS (b) Post EELS

Figure 4.16: HAADF image taken before a) and after b) EELS quantification. Contamination can be seen to have built up in the time it takes to perform one scan.

yield of born-rich nanowires some of which are multiple twinned. This method of producing the nanowires can be viewed as an improvement of the previous procedure which gave a simple method of producing the five fold twinned nanowires because of the ease of observing the nanowires.

The nanowires grown on the powder sample are sporadic whilst the silicon wafer is uniform over a large area, i.e. you can look at any part of the silicon wafer and observe growth sites, but with the powder sample they must be found first, this can be time consuming. Both samples are produced using the same simple reaction but the remote growth has a greater potential for harvesting the nanostructures because they all grow on a flat surface. When the nanostructures are dispersed in alcohol there is some debris, but much less debris than that occurs when the powder sample is used.

Although there are many benefits to this system of producing boron rich nanowires there are also downsides. Because of the surface destruction there is a possibility that some of the nanowires seen in the SEM micrograph are silicon nanowires. Due to the surface destruction of the silicon wafer there is a chance that some of the wires are doped with silicon. The presence of amorphous and single crystalline boron carbide nanowires as well as the multiple twinned nanowires indicates we still have work to do to be able to fully understand and control the growth of these boron rich nanostructures with their unique morphologies.

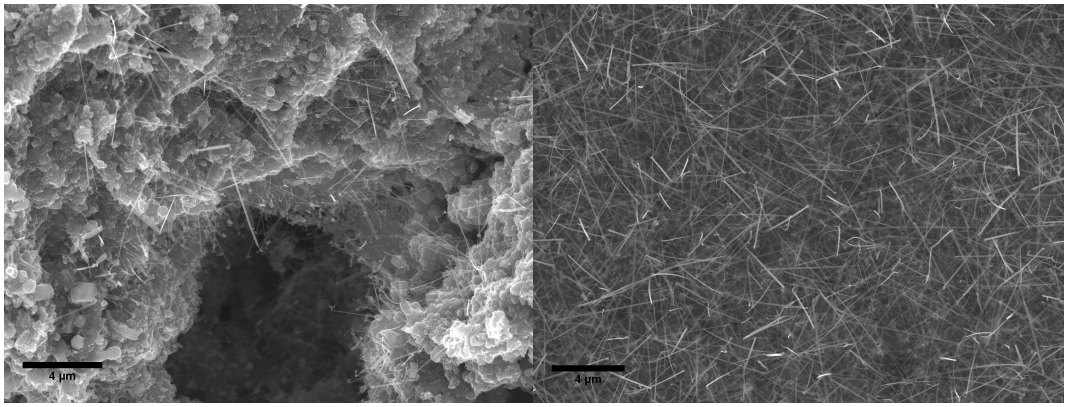

(a) (b)

Figure 4.17: These images show the difference between a) the earlier method when the nanowires are grown in the powder pellet and b) when the growth happens on a silicon substrate.

4.3 The role of the iron precursor layer.

In other VLS processes [21] they have demonstrated that the process can be controlled by the catalytic metal. Now that we have shown that the multiple twinned boron carbide nanowires can be grown remotely on a silicon wafer covered with iron a study to compare the system with other accepted VLS systems will be performed.

To prove that the iron was essential for the growth of the nanostructures on the silicon an experiment was designed to isolate regions on the silicon wafer covered by iron from areas with no iron on the silicon. If iron is essential for the growth of the nanostructures then the nanostructures will not grow on the regions free from iron.

The silicon wafer was prepared in the same manner as described previously in section 4.2.1, using the HiTUS sputtering system, except this time a quarter of the wafer was covered with tape before it was sputtered. This was done to keep the surface free from iron.

The samples were grown using the same method previously used to grow the sample section 4.1 with the addition of a silicon wafer. The samples were analysed in an FEI SEM with NORAN system elemental X-ray analysis.

The interface between the region of silicon covered in iron and the region free from iron is clearly visible figure 4.18. The interface is a straight line as would be expected from using a piece of tape to mask the surface. Nanostructures can be seen on the right of the image and the silicon substrate is still visible on the right.

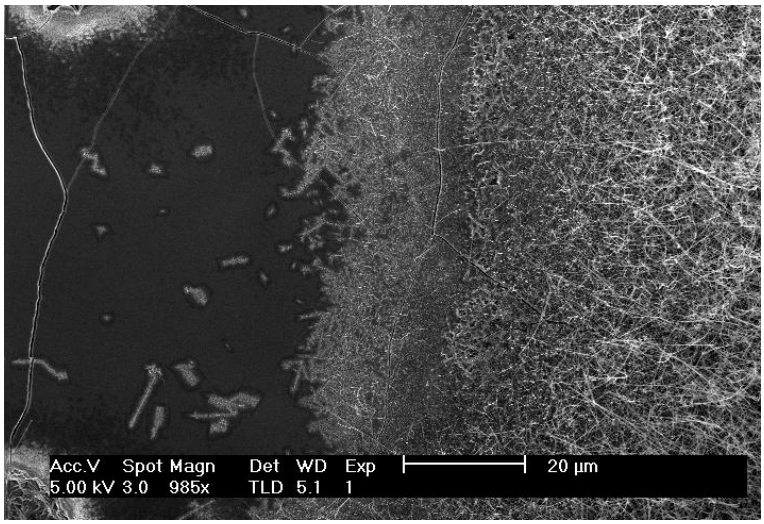

Figure 4.18: SEM image of the interface between the iron covered region (right of image) and the region free from iron (left of image).

The surface of the masked area of silicon is free from nanostructures figure 4.18. This is consistent with the fact that the iron is responsible for the presence of the nanostructures. This information allows the growth of the nanostructures to be targeted to specific areas of the sample.

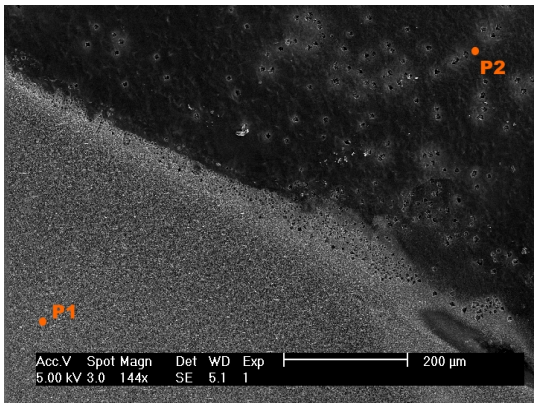

Figure 4.19: The points marked P1 and P2 at which the EDX measurements were made, on either side of the interface.

To confirm the presence of boron rich nanostructures on the area covered with iron EDX analysis was done. We expected to see peaks for boron, carbon and iron on the region covered with nanostructures and only peaks for silicon and oxygen on the masked region. A series of EDX spectra obtained from the points in figure 4.19 are displayed in figure 4.20-21. The inserts in the figures are of the entire energy spectrum and have been plotted with the counts axis on a log_{10} scale in order to show that there is nothing above the noise threshold.

At an accelerating voltage of 5kV we can see the peaks for boron and carbon these are from the nanostructures grown on the surface of the region covered with the iron. Also visible are the peaks for oxygen and silicon. These can

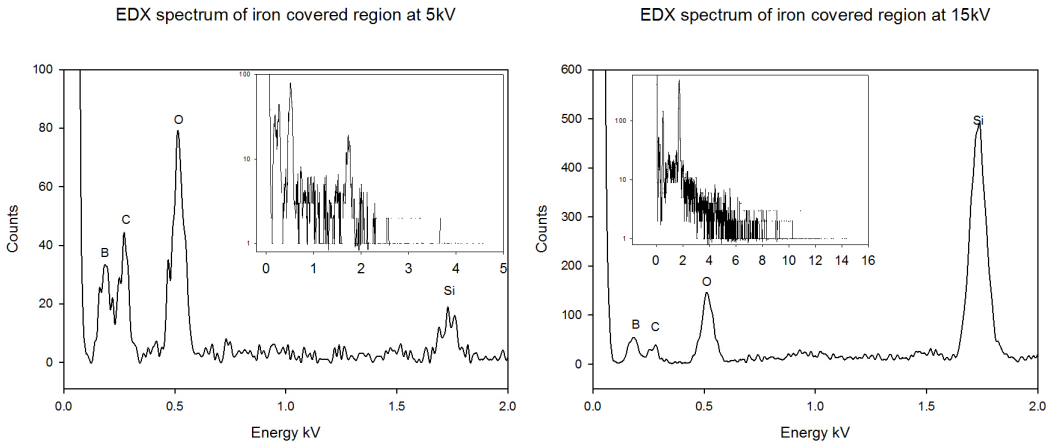

(a) (b)

Figure 4.20: EDX of silicon surface where nanowires have grown showing peaks for expected elements B, C, O and Si at a)5kV and b)15kV. Note the absence of peaks for iron (L_α 0.71 keV or K_α 6.4 keV).

be explained by the presence of an oxide layer on the silicon upon which the nanostructures are grown. Although it must be noted that there is a possibility that there are contributions from silicon oxide nanowires that have grown alongside the boron rich nanostructures as discussed previously. Unexpectedly there is no peak for iron on either of the spectra. Looking at the full spectra obtained (insert of figures 4.20) do not show a peaks for iron which would be expected at either L_α 0.71 keV or K_α 6.4 keV.

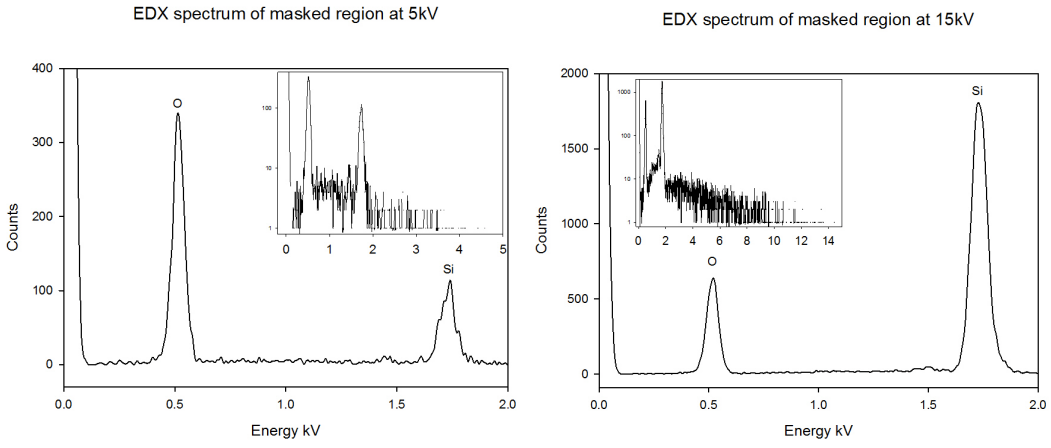

(a) (b)

Figure 4.21: EDX of surface where no nanowires have grown showing peaks for expected elements B, C, O and Si at a) 5kV and b) 15kV.

These spectra are from the region of the sample that was free from iron. We see only peaks for oxygen and silicon. The absence of boron on the surface that is free on iron is consistent with expectations as the iron is an important component of the growth of the boron rich nanostructures.

This is consistent with the statement that the iron is required for the nucleation of the nanostructures, but iron is not found on the sample after it has been fired [30].

Cui *et al* demonstrate that VLS growth is able to control the diameter of the wires by varying the size of the catalytic metal drops. It would be interesting to know if our system allows a similar control.

In order to investigate how the iron affects the growth of the nanostructures an experiment was designed to see how the thickness of the sputtered iron layer would affect the distribution of the diameters of the nanostructures.

The samples were produced using the same technique described earlier in section 4.1 but the samples were grown with different thickness iron layers. The range of thickness's used was 20, 30, 40 and 50 nm.

SEM micrographs of the samples were obtained from random positions on the surface of the wafer and analysed to observe any trends in the width and the density of the nanostructures. A representative selection of the images taken is shown below in figure 4.22.

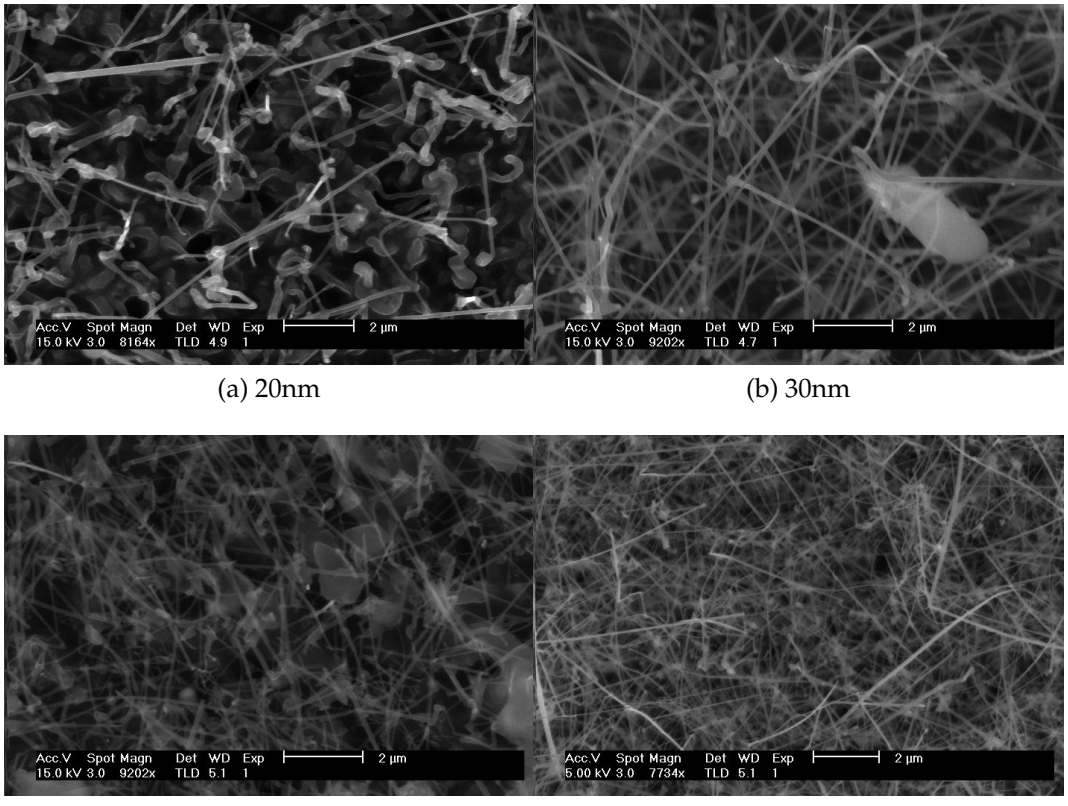

(a) 20nm (b) 30nm

(c) 40nm (d) 50nm

Figure 4.22: Images taken at random positions of nanomaterials grown on the surface of silicon wafers with different thickness of iron.

This series of images from the four different samples produced show the chang-

ing density of the nanostructures. The images were analysed to find the number of wires per μm^2. This was done by counting the number of wires present in a known area of the sample.

Thickness of iron layer	Number of wires per μm^2	error
20 nm	0.36	0.03
30 nm	1.01	0.03
40 nm	1.18	0.04
50 nm	1.41	0.30

Table 4.2: Density of nanowires grown for different iron thickness.

The same images were also analysed to determine the distribution of diameters of the nanomaterials produced. The results are displayed in [Figure 4.21].

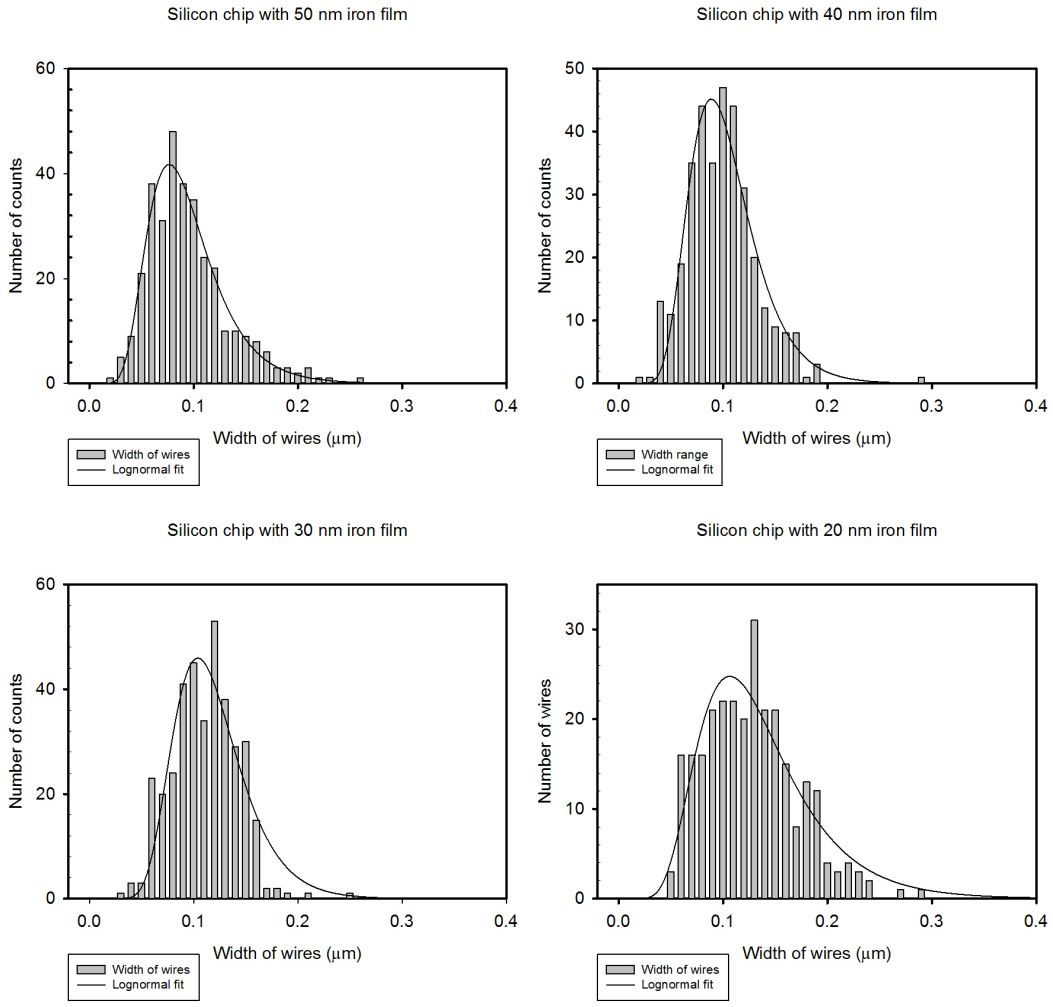

Figure 4.23: Series of graphs showing how the diameters of the nanowires grown vary with different thickness of catalyst layer.

The distributions in figure 4.23 show that the average thickness of the nanostructure produced via this method remains roughly constant.

We can use these results to state that we can grow a higher density of nanostructures with a thicker film of iron, but the thickness of the iron layer does not have any great effect on the thickness of the nanomaterials produced as displayed in figure 4.24.

The increased density is likely due to the thicker layer of iron forming a greater number of droplets when the layer is thicker. However the thickness of the iron layer does not affect the size of the droplets that are formed. The size of the droplets is more likely dominated by other factors such as the temperature.

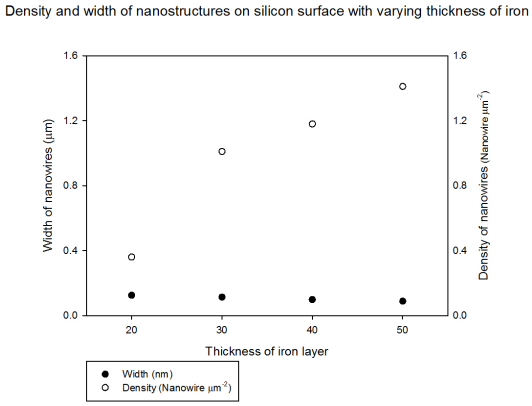

Figure 4.24: Comparison of how density and Average width of nanomaterial change with different thickness of iron layer on the silicon wafer

4.4 What happens to the iron?

Previously it has been noted that there is an absence of iron in the chemical analysis. This could be due to the detector not being sensitive enough to register the amounts of iron in the sample. To test whether this was the case, iron coated silicon wafers that had not been fired were analysed. The scans were performed at 5 kV and 15 kV, and all the scans were able to detect some level of iron from all of the samples. Figure 4.25 is one such scan on the wafer with the lowest level of iron coating (20nm thick layer). This suggests that the level of iron present in the sample after it has been fired is less than the initial levels because it is not detected.

The iron may be able to evaporate from the sample in some way. By looking at the compounds present in the reaction it may be possible for the iron to form an iron boride compound which may have a melting temperature of the order of 1300°C [39]. The literature states that one of the main products of the reaction in powder is FeB [27].

In experiments on Carbon nanotubes it has been shown that it is possible for iron to permeate into the silicon and sit at the interface between the silicon and

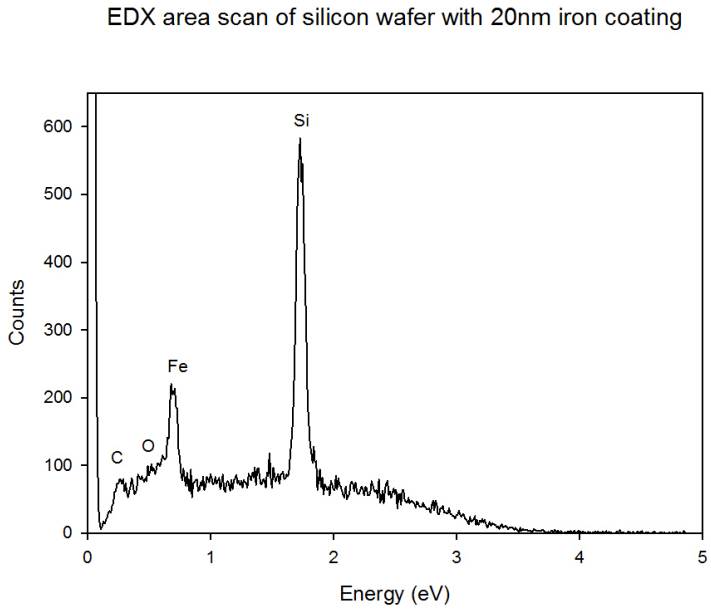

Figure 4.25: Test to make sure the EDX is sensitive enough to the levels of iron

the silicon oxide [40]. If this mechanism is present in our system then the iron may exist at the interface betwin silicon and silica.

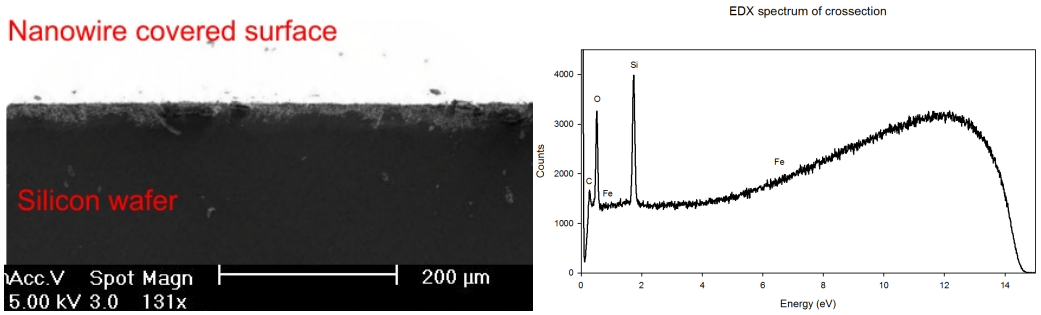

(a) (b)

Figure 4.26: a) Cross section view of the silicon wafer broken in half a) and EDX of the oxide layer b).

The cross section of one of the silicon wafers was examined to see weather the iron could be detected at the bottom of the oxide layer.

In figure 4.26 a) we can see the cross section of the wafer. When EDX figure 4.26 b) was performed on the cross section no peaks for iron were seen. Although the spectrum does have a higher background at higher energies there is still an absence of peaks at the expected position.

Because the levels of iron are relatively small and the growth is done under gas flow, the iron may simply be able to evaporate even though its melting temperature is higher than the reaction temperature.

EDX analysis was performed on individual nanowires in the TEM. Figure 4.27 a) shows a dark region in the droplet structure of the nanowire, This shows that there is iron present in the tips due to Z contrast. however the dark region is only part of the structure, and the rest is likely to be an oxide according to the EDX scan in figure 4.27 b). The EDX scan in figure 4.27 b) also shows that there is silicon present in the wires. The silicon is likely to have been incorporated from vapour produced by the destruction of the surface by the high temperature of the reaction, or as an impurity present in the chemicals used in the reaction that produces the boron rich gas.

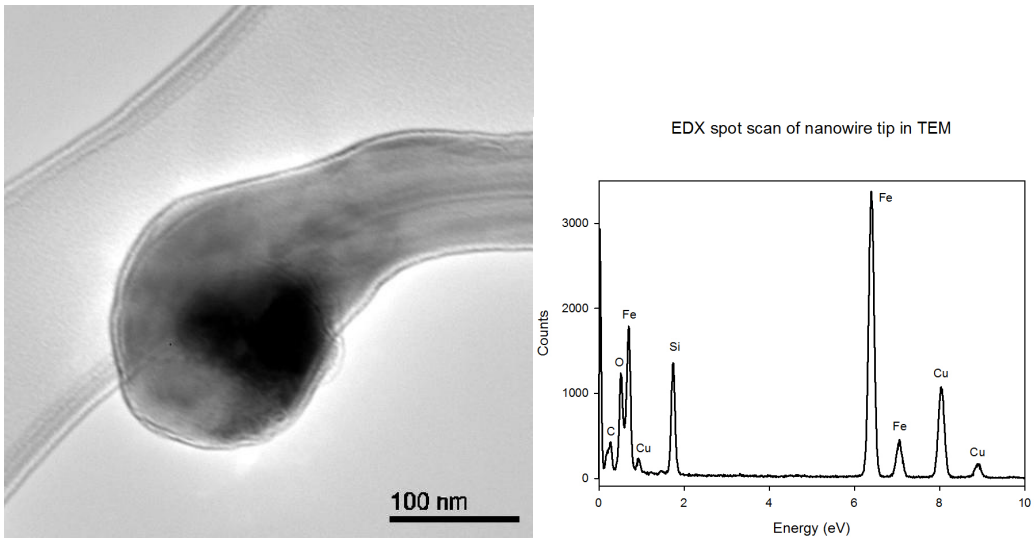

(a) (b)

Figure 4.27: TEM image of nanowire tip a). EDX analysis performed on the nanowire tip b).

Work by Jiang [30] has shown that the nanowire can be wetted by the iron at temperatures of 1300°C and be incorporated into it during growth. Even though the iron is no longer present a droplet structure still exists but is mainly an oxide of boron. His work shows that the growth of the nanowires is not reliant on the presence of iron. My work has shown that iron is essential for nucleation of the nanostructures, and the low levels of iron suggest that it is not essential for growth but it is present in the nanostructures. It should be noted that the iron may still have a role, but it has not been possible to determine it during this work.

Chapter 5

Conclusions.

> The whole of science is nothing more than a refinement of everyday thinking
>
> Albert Einstein

5.1 Conclusions.

This work contains an account of how the conditions were varied in order to explore the growth of boron rich nanostructures. To conclude, the findings of this work are summarised in this chapter.

Firstly we have shown that the multiple twinned boron rich nanostructures initially grown in a powder, can be grown via a Vapour based method. This was done by having the nanostructures grown remotely from where the boron rich gas was produced in the powder pellet. Doing so removes the possibility of any solid state reactions. Whilst examining the sample an assortment of nanostructures were observed, including those that exhibit the characteristics of being multiple twinned.

We have demonstrated that the iron is important for the nucleation of the nanowires. This was done by having regions free from iron on the surface of a silicon wafer. The areas kept free form iron were free from nanostructures. This suggests the presence of a VLS based method. Our demonstration also shows that we can target the growth of nanostructures to desired locations by using masks when depositing the iron.

The role of the iron layer was investigated and it was found that by varying the thickness of the layer we could vary the density of the nanostructures. A thicker layer of iron would give a higher density of nanowires than a thinner

layer of iron. The average diameter of the nanomaterials seems to remain independent of the thickness of iron layer. The diameter is most likely to depend on the experimental conditions.

Chemical analysis via EDX analysis of the nanostructures grown show that the samples contain boron, carbon, oxygen and silicon. The silicon is from the wafer upon which the sample is grown, and there is a surface oxide that would account for the large amount of oxygen present. This leaves boron and carbon as foreign elements which have arrived at the sample during the growth process. This evidence points towards the presence of boron carbide nanowires. Although it is possible that there are boron suboxide, and silicon nanowires present.

EELS on several nanowires gives a large variety of chemical compositions. No oxygen was detected on the wires sampled, they were all made of carbon and boron. The ratios calculated by the software vary from 36% to 77% boron. This variation may be explained by the build up of contaminant carbon on the surface of the wire. There is also a possibility that the ration of boron to carbon is variable [41]. The fine structure of the boron edge compares well with the edge for boron carbide. These results point to the sample being predominantly boron carbide.

Analysis of diffraction patterns from TEM shows us that we have a variety of wires present in the sample. Diffraction patterns were obtained for twinned nanowires, single crystal nanowires and amorphous nanowires. Simulations confirm that the boron carbide structure for the single crystalline nanowires. Dark field imaging was used to show that different well defined region of the nanowire are responsible for the twinning diffraction pattern. Comparison to simulations confirm a cyclic twinning structure of boron carbide is present in some of the wires.

My experiments seem to suggest that the iron may not be needed for continued growth after the nucleation of the nanowires, because the levels of iron have fallen below the detection limit of the EDX on the SEM. The iron was detectable before the Iron coated silicon wafer has boron rich nanomaterials grown on its surface. The iron may form an iron boride compound in the presence of the boron rich gas. Iron boride has a melting point of the order of 1300°C [39]. This is the same temperature as the reaction temperature of the furnace, and as the furnace is at this temperature for an hour under gas flow then the iron may evaporate and travel out of the system. This would leave an oxide assisted growth mode to then dominate. However this is not confirmed in this work.

5.2 Further work.

Now we have a greater understanding of how the product of the process varies at one temperature, the same investigation should be conducted at different temperatures. Special attention should be given to the presence of the iron at temperatures below 1300°C this may help to confirm what happens to the iron, i.e. does it evaporate as it is not at a close enough temperature to its boiling point. If the iron is present at lower temperatures does its presence cause a variation in the type of nanostructures grown?

Using a mixture of powders to produce boron rich gas is not an elegant method, for commercial applications it would be desirable to have a boron rich gas such as diborane as used by Otten *et al* [26]. This method should be investigated to ensure that the twinned nanowires are present.

Some of the potential uses of boron rich material depend on the mechanical properties of the nanowires. An investigation of properties such as the Young's modulus and the electronic properties and how they vary for different wires. Preliminary investigations have shown that it is possible to force nanowires to oscillate using a method developed by Scruton [42]. A nanomanipulator is moved to be in close proximity of a nanowire tip. An oscillating electric field is applied to the manipulator. At the correct frequency the nanowire will resonate. The resonant frequency can then be used to calculate the Young's modulus of the nanowire. These graphs in figure 5.1 show the resonance curve for two different nanowires grown with a different thickness of iron precursor.

Using the formula below which comes from simple beam theory.

$$E = 16\rho\left(\frac{2\pi f_0 L^2}{\beta_0^2 D}\right)^2 \tag{5.1}$$

where ρ is the density, L is the length of the nanowire, D is the diameter of the nanowire, f_0 is the natural frequency, β_0 is an eigenvalue for a cantilevered beam (= 1.875) and E is the elastic modulus of the nanowire.

Nanowire 1 has $D = 89nm$, $L = 26.9\mu m$ and $f_0 = 1.05GHz$. These values give an elastic modulus of 614.7 GPa. This value is greater than the $4.48x10^1 1Nm^-2$ = 448 GPa experimentally determined for bulk boron carbide[43]

Nanowire 2 has $D = 362nm$, $L = 39.1\mu m$ and $f_0 = 0.66GHz$. These values give an elastic modulus of 201.56 GPa. This value is consistent with values obtained for silicon nanowires [44]. However this value is also what was found for curved crystalline boron nanowires [4].

The result for wire 1 in particular indicate that an improvement in the Young's modulus from bulk boron carbide. However a more systematic investigation is required in order to confirm this.

These preliminary results indicate that this method of growing nanowires will lead to an improvement in the elastic properties over bulk boron carbide. If this technique is to be used to obtain results I would recommend a refinement of the technique so more points can be measured more accurately.

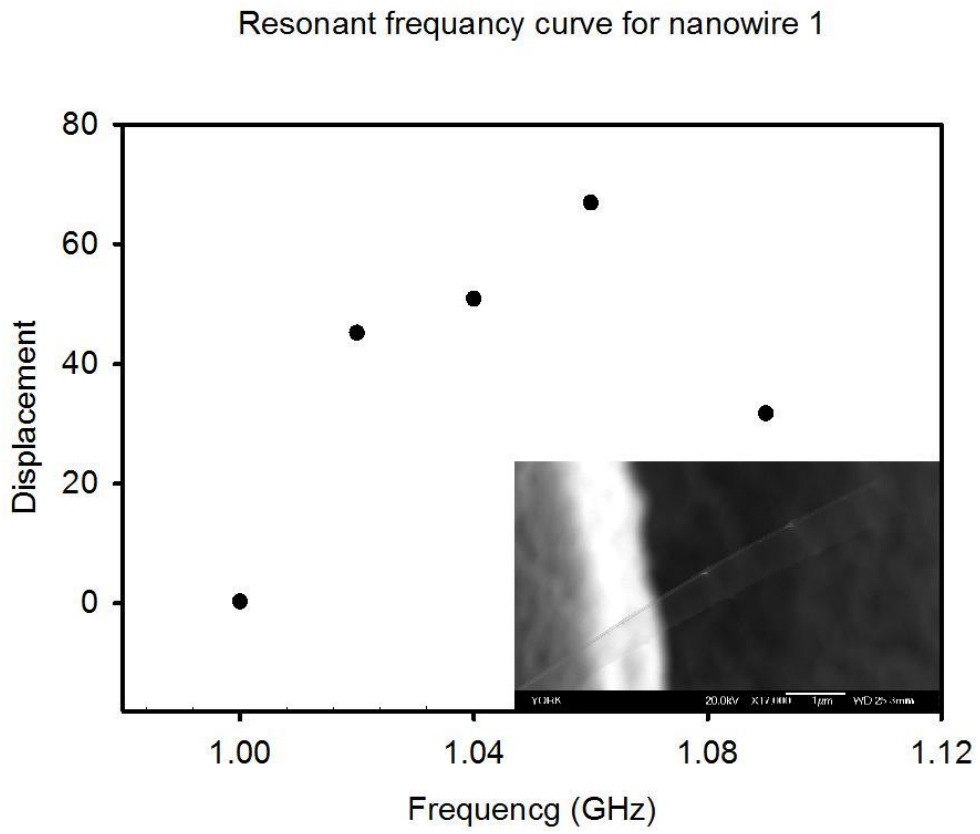

(a)

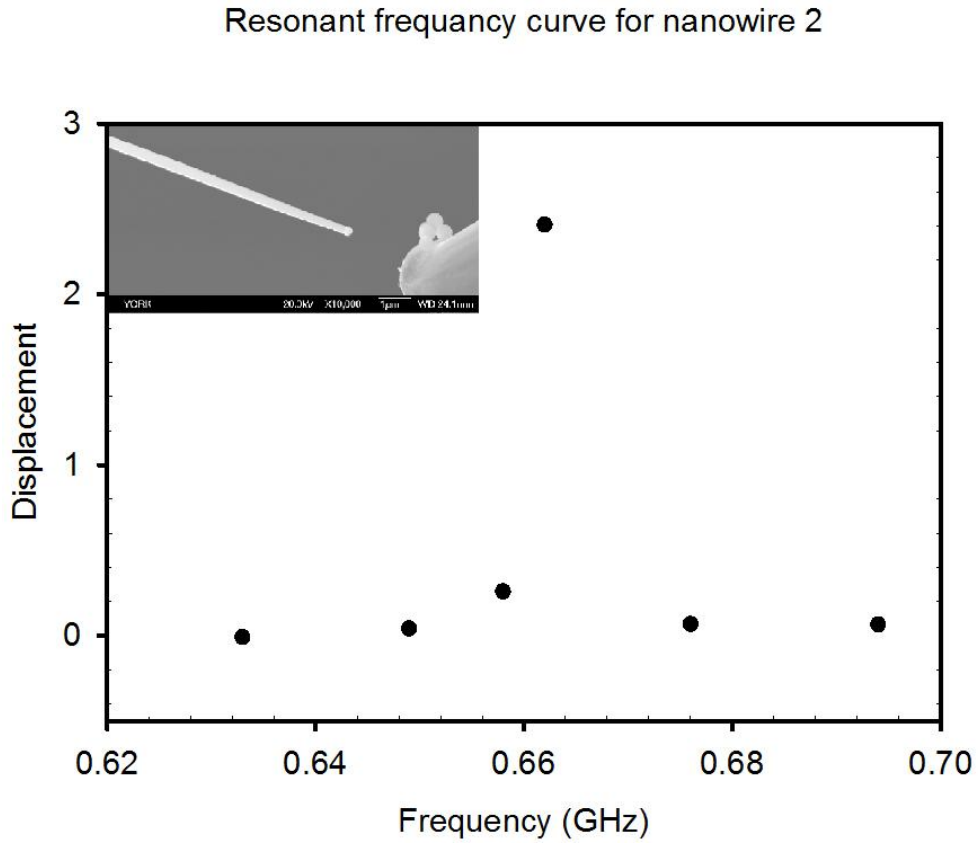

(b)

Figure 5.1: These figures show the resonance curves of nanowires grown under different conditions. Note the displacement is on an arbitrary scale.

Chapter 6

List of Abbreviations

VLS	Vapour Liquid Solid.
CVD	Chemical Vapour Deposition.
SEM	Scanning Electron Microscope.
TEM	Transmission Electron Microscope.
STEM	Scanning Transmission Electron Microscope.
EELS	Electron Energy Loss Spectroscopy.
ADF	Annular Dark Field.
HAADF	High Angle Annular Dark Field.
EDX	Energy Dispersive X-ray.
JEOL	The JEOL Company. Manufacturer of Electron Microscopes.
FEI	The FEI Company. Manufacturer of Electron Microscopes.
MKS	The MKS Company. Manufacturer of Gas control systems.
MFC	Mass Flow Controller.
HiTUS	High Target Utilisation Sputtering.
SOP	Standard Operating Procedure.

Table 6.1: List of abbreviations.

Appendix A

Appendix A.

This appendix contains the operation manuals and health and safety procedures put in place during this work.

These are included so that they are able to be referenced and will greatly aid understanding of operations for any trying to replicate this work.

Quick Operation of High Temperature Furnace

This document is designed to offer a quick start in the use of the high temperature furnace. This should be read in conjunction with the relevant manuals and is not a substitute for the manuals. Specifically this can be used by project students to use the furnace quickly and safely.

Warning

- The furnace is capable of high temperatures, so care must be taken when working near the furnace when it is running.
- Parts of the furnace are made of ceramic. These brittle parts can be easily damaged by slight knocks. The ceramic components are also expensive to replace.
- Wear gloves at all times when in contact with the furnace. Doing so will protect your hands from any debris left in the vessel and prevent the oily smuge on your hands damaging the ceramic components.
- Make sure you have filled out a risk assessment, and have read all the appropriate Materials Safety Data Sheets (MSDS) for the compounds you are going to use, the likely intermediates and final products (including gaseous phases).

Before you begin.

1. Make sure the furnace is cold. Do not attempt to open the furnace when it is warm. The temperature of the furnace can be checked by turning on the Furnace Power Supply on the wall, the internal temperature of the furnace is displayed on the Furnace Readout [Fig.1].
2. Make sure the Heat ON button on the Furnace Control Panel is in the OFF position. The Elements Isolated should be lit when you turn on the furnace [Fig.1].
3. If the weather has been cold there is a chance that the exhaust pipe may be blocked by ice. If the temperature outside has dropped below zero recently then check the pipe outside. Access to the courtyard is through the doors at the end of DF wing near the engineering workshop.

Not all steps mentioned have to be followed. The steps used depends on the specific needs of your experiment.

Operation of the furnace.

4. Remove both End Plates and the Heat Shields [Fig.3]. Place them safely on the bench (so that they cannot roll off).
5. Use the wooden Meter Rule to push the Inner Tube so that it is at one end of the Outer Tube [Fig.3]. The Meter Rule can be found hanging on the wall near the gas bottles. Please return to its place after using [Fig.1].
6. Place the Reaction Boat [Fig.4] carrying your sample inside the Inner Tube and position using the Wire [Fig.1] to push the Reaction Boat so that it is roughly 270mm inside the Inner Tube [Fig.3].
7. Use the wooden Meter Rule to push the inner tube approximately 400mm inside the Outer Tube.
8. Put the Heat Shields back into the outer tube [Fig.3].
9. Place the End Plates back on the flanges and tighten [Fig.3]. The nuts should be sequentially tightened a quarter turn each until finger tight.
10. Enter your program for the furnace. Details on how this is done are described in **Appendix 1**. These instructions are taken from the manufacturer manual.
11. Make sure all valves (V1-V4) are closed (perpendicular to the pipe) [Fig.1].
12. Turn on the power to the Gas Control Unit [Fig.1]. The switch is located on the front of the unit
    a. The first screen shows the flow (FL1) and the setpoint (SP1) for MFC1 [Fig.1].
    b. The second screen shows the flow and setpoint for MFC2 [Fig.1]. Navigation between these two screens is done via the up and down arrows.
13. Pump the system. The pump can be found on the side in the sample preparation area of the lab.
    a. Attach the pump inlet to the furnace via V3 [Fig.1].
    b. Attach the pump outlet to the exhaust pipe leading outside.
    c. Open valve V3 [Fig.1].
    d. Turn on the pump.

e. Pump the system until the pressure is constant. Use the Pressure Gauge to check this [Fig.1].
f. After the vessel is pumped down close V3 and turn the pump off [Fig.1].
g. Disconnect the pump and return to its place in the lab.

14. Flush the system.
    a. Open the argon gas bottle and open the Regulator (clockwise) so that the outlet pressure is 1 bar [Fig.2].
    b. Use the arrow buttons on the Gas Control Unit to change SP1 to 800 sccm [Fig.1]. To change the SP press the right arrow an underscore will appear underneath one of the digits. Use left and right to select the desired digit and then use the up and down buttons to change the numbers. Press enter to confirm your selection. The underscore will disappear when your selection is confirmed.
    c. Press the ON button on the Gas Control Unit [Fig.1].
    d. Slowly open Valve V1 [Fig.1].
    e. Once the Pressure Gauge reads 1000 bar. Wait a further minute and then open Valve V4 [Fig.1].
15. Depending on the sensitivity of your experiment to atmospheric gasses you may want to repeat the pumping of the system several times.
16. Put the Heat ON switch in the ON position. The Isolate Elements light should now be off [Fig.1].
17. Now start the furnace program running.
18. Change to use the other Gas bottle.
    a. Open the gas bottle. Open the regulator (clockwise) so that the outlet pressure is 1 bar [Fig.2].
    b. Use arrows buttons on the Gas Control Unit to change SP2 to the desired flow rate [Fig.1].
    c. Open Valve V2 [Fig.1].
    d. Close valve V1 [Fig.1].
    e. Change SP1 to zero.
19. Once the furnace is cooling put the Heat ON in the OFF position. The Isolate Elements light should now be lit [Fig.1].
20. When the furnace is cool.

a. Change SP1 and SP2 to zero if they are not already at zero. Make sure that the Regulators [Fig.2] are closed (anticlockwise) as far as it will go and that the gas bottles are closed.
b. Close all valves (V1-V4) [Fig.1].
c. Press the OFF button on the Gas Control Unit [Fig.1].

21. Turn off the power to the Gas Control Unit [Fig.1].
22. Turn off the Furnace Power Supply [Fig.1].
23. The End Seals can now be opened and the Reaction Boat removed from the furnace [Fig.4]. By following steps 5. and 6. Use the Wire to carefully pull out the Reaction Boat with your sample inside.

Appendix.1

BASIC OPERATION/PROGRAMMING
EUROTHERM 2416 PROGRAMMER

Use as a PID Setpoint Controller.

Press either the 'UP' ▲ or 'DOWN' ▼ buttons to adjust the lower displayed reading to indicate the required setpoint. The furnace will heat up at its fastest rate to the setpoint once the furnace door is closed and the 'HEAT ON' switch is moved to the (1) position.

Frequently, it is undesirable to allow the furnace to heat up the load at the fastest rate, and a series of controlled temperature ramps and dwells at specific temperatures may be required.

Setting a Programme.

1. Decide whether the programme ramps are to be in °C per minute or °C per hour.

2. Decide whether the required dwell times are to be in minutes or hours. These two parameters are adjusted early on in the sequence, and apply to all ramps and dwells in the set programme.

3. Ensure that the 'HEAT ON' switch is OFF (O) position. This prevents unwanted heating of the furnace during setting up of the programmer.

4. The programme is tamper protected and access to the programme setting is by password.

5. The default password as supplied is (number) 1.

6. Switch on the instrument and allow it to stabilise after its self test routine.

Method

1. Press the left hand 'PAGE' button several times until 'ACCS LIST' is displayed.

2. Press the second left 'SCROLL' button once to display 'CODE 0'.

3. Press the 'UP' ▲ button once to change the lower display to 1.

4. 'CODE PASS' will now be displayed.

5. Press second left 'SCROLL' button once to show 'GO TO OPER'.

6. Press 'UP' ▲ button once to change display to 'GO TO FULL'.

7. Press left button 'PAGE' several times to show 'PROG LIST'.

8. Press second left 'SCROLL' button to show 'Hb OFF'.

BASIC OPERATION/PROGRAMMING
EUROTHERM 2416 PROGRAMMER

Holdback is a feature which allows the programme to stop and wait for the furnace to "catch up" with the programme if, for example, too fast a heating or cooling rate has been set in the programme.

To set the holdback, it is usual to set this as 'BAND' and then to set the number of °C above and below the setpoint, outside of which the programme will stop and wait for the furnace temperature to rise or fall to within the set band.

Thus, for any given load, the holdback will ensure that the load will remain at the required temperature **+** or **-** the holdback figure irrespective of any programme ramp rate setting.

9. If holdback is required press either the 'UP'▲ or 'DOWN' ▼ button until 'bAnd' is displayed.

10. Press second left (scroll button) to display 'Hbu' and adjust the lower reading using the 'UP' or 'DOWN' button to change the lower display to the required holdback band.

11. Using the scroll button press once to display 'rmPu' and then depress either the 'UP' ▲ or 'DOWN' ▼ button to select secs, mins or hours. This will then enable further setting to give °C per minute/hour/second.

12. Press scroll once again to display 'dwLU' and adjust the bottom display to read either sec/min/hour as required for the dwell periods.

13. Press scroll to read 'CYC.n.'. The lower figure will indicate the number of times the programme will cycle before ending. Adjust the figure using 'UP'▲ or 'DOWN' ▼ buttons as required.

14. Press scroll button to indicate 'SEGn1'. This will then be the first segment in the program.

15. Press scroll button to show 'TYPE RMPr'. This will allow a setting of °C/unit of preset time e.g. if in (11), minutes was selected, then the ramp setting will be in °C per minute.

16. Press scroll again to indicate the level to which the ramp should go. Adjust the lower reading using the 'UP/DOWN' buttons to show the desired level.

17. Press scroll again to show 'rATE.00.' Adjust the lower reading to show the desired ramp rate.

18. Press the scroll button again 'SEGn2' shows. This will be the next segment for adjustment: If you wish to re-adjust segment 1, simply press the down button, then the scroll button to access the required parameter.

BASIC OPERATION/PROGRAMMING
EUROTHERM 2416 PROGRAMMER

19. Assume that the segment 2 is to be a dwell at the target temperature. Press the scroll button to show 'tYPE DWELL'. If 'DWELL' doesn't show, use the 'UP/DOWN' button to change the bottom display.

20. Press 'SCROLL' - 'durXX' will show. Adjust lower display to show the required dwell period. This will be in units of time as preset in (12).

21. Scroll will now show segment 3. Assume this is to be the end of the program and the furnace should cool down at its natural rate.

22. Scroll the 'TYPE XX' and adjust lower display to read 'END'.

23. Scroll to show 'END RSET'. END can be a dwell or a reset. Select reset. Reset exits program mode and reverts to standard control mode.

24. **If the furnace is to cool to ambient temperature then the basic setpoint as described in** "Use as a PID setpoint controller" **MUST** be set to zero.

25. If other ramps or dwells are required in the program, simply enter the ramps and dwells in sequence as per the foregoing instructions.

    8 segments are available for use as ramps or dwells in any sequence.

To Run a Program.
Press the small button marked 'RUN HOLD'. Run will illuminate.

To Hold a Program at any Point.
Press the 'RUN HOLD' whilst in a program. 'HOLD' will illuminate.

To Reset a Program
- Press 'PAGE' button several times to show 'ACCS LIST'.
- Press 'SCROLL' to show 'GOTO FULL' (adjust if necessary) with 'UP/DOWN' buttons.
- Press 'PAGE' button to show 'RUN LIST'.
- Press 'SCROLL' to show 'STAT OFF' (adjust with 'UP/DOWN' buttons as necessary.

Note: Should no key operation be performed within 45 seconds, the indication will revert to 'normal' indication of setpoint and measured temperature. However, it will not be necessary to re-enter access code number unless the instrument has been turned off. Pressing the 'PAGE' button will enable re-access to 'PROGLIST' and scrolling through the list will return to the required parameter for setting.

Fig.1

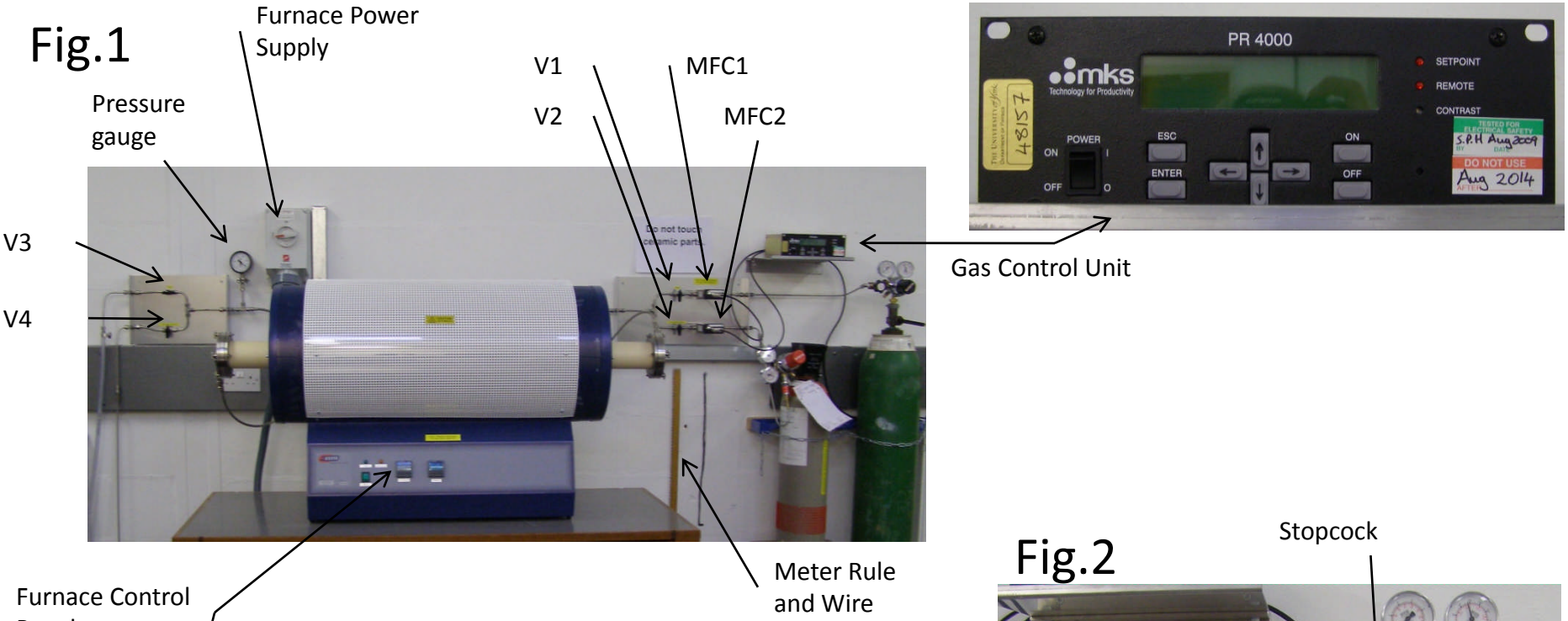
Furnace Power Supply
Pressure gauge
V1
V2
MFC1
MFC2
V3
V4
PR 4000
SETPOINT
REMOTE
CONTRAST
Gas Control Unit
Furnace Control Panel
Meter Rule and Wire
Elements isolated
POWER
ELEMENTS ISOLATED
OVER TEMPERATURE
Run Button
Heat ON
Furnace Readout

Fig.2

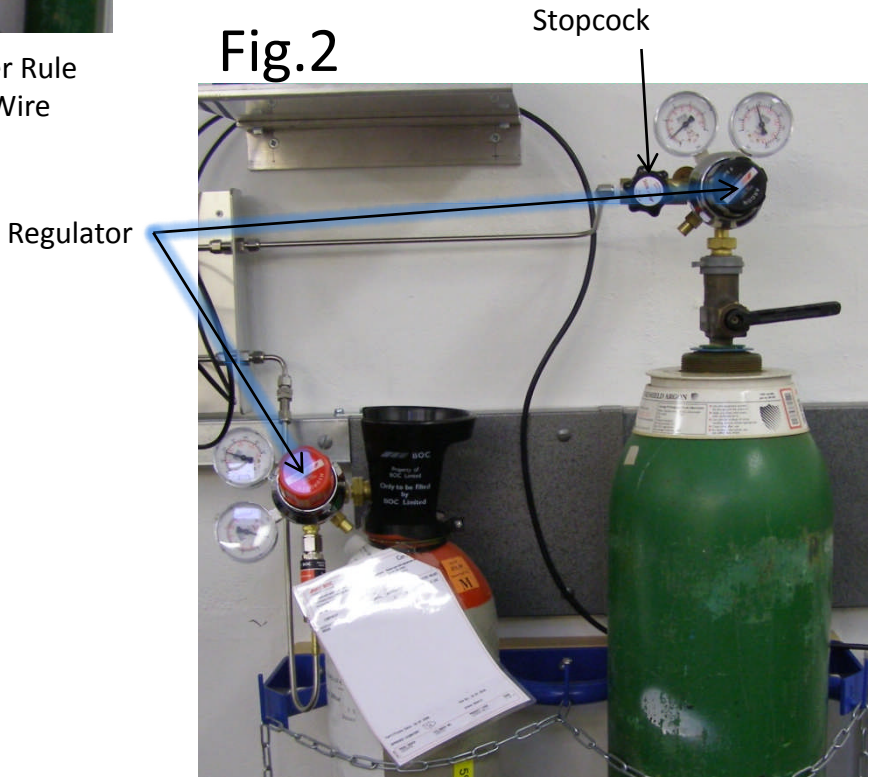
Stopcock
Regulator

Fig.3

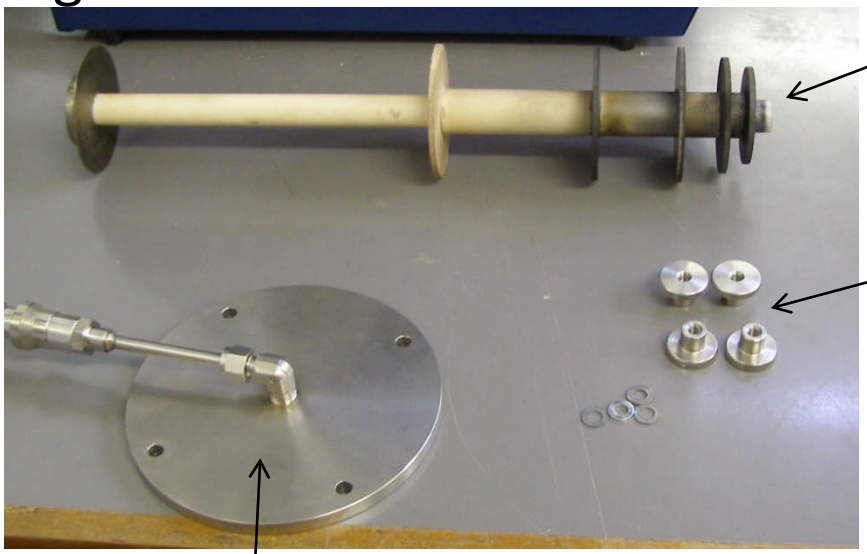
Heat Shield
Nuts
End Plate

Fig.4

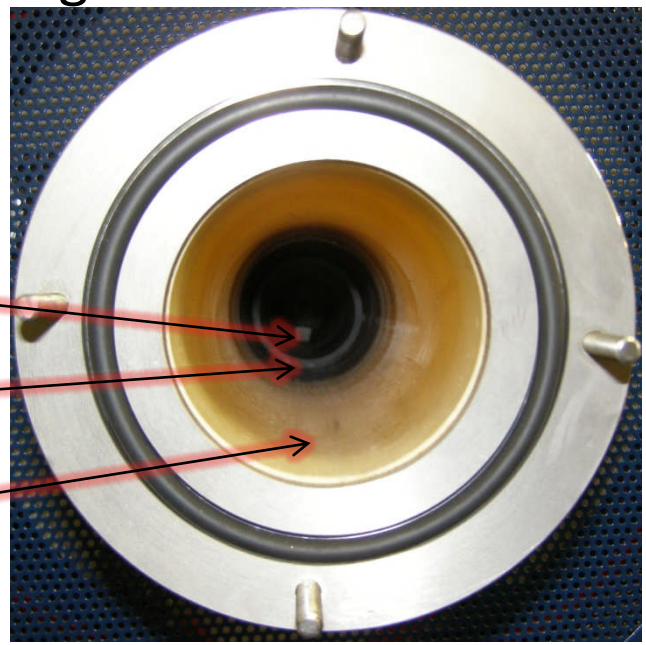
Reaction Boat
Inner Tube
Outer Tube

Standard Operating Procedure for high temperature furnace.

This Standard Operating Procedure **ONLY** covers the procedure for producing boron rich nanostructures using Boron, Iron(II\III) Oxide, Barium Oxide and Glycerol. If you want to use **ANY OTHER MATERIALS** to produce nanostructures a new Standard Operating Procedure should be approved. The Standard Operating Procedure should cover any products and intermediate compounds formed in the reaction and the correct method of handling and disposing of the materials produced. Any materials that are potentially hazardous should be noted in particular.

Safety.

Before using any of the materials you must have read the Materials Safety Data Sheet (MSDS) for all compounds.

You should understand and comply with any safety procedures mentioned in the risk assessment.

You should not attempt to operate the equipment unless you are familiar with the correct procedure as detailed in the manual. Doing so may result in damage to the apparatus and a potentially risks to safety.

When handling the products:

-Wear gloves at all times and wash your hands afterwards.

Reaction products and intermediate compounds.

This reaction is designed to produce:

- Boron suboxide, Boron carbide.

However these compounds and intermediates may also be formed:

-Iron Borate, Iron Oxide, Boron Oxide, Colemanite, Boric acid.

Boric acid has a pH of 4 in a saturated aqueous solution.

Disposal of materials.

To dispose of materials they should be sealed in a suitable container, clearly labelled and taken to Chemistry stores on a Monday or Wednesday afternoon (1:30-3:30pm). The technicians will arrange for their waste disposal contractors to dispose of it safely.
The waste will be treated as chemical solid waste.

An internal waste transfer note should be completed (attached at rear) and handed over with the material for disposal. A copy of the internal waste transfer should be retained for our records.

Internal waste transfer note also available online at:
http://www.york.ac.uk/admin/hsas/safetynet/Waste%20Management/Internal%20Waste%20Transfer%20Note%20(VS%201.1%20-%20May%2008).pdf

Chemistry stores can be contacted on extension 4547. The waste disposal technician is Owain Samuel.

DO NOT MAKE COPIES OF THIS DOCUMENT

Name: _____ Date: _____ Experiment ID: _____

Complete a risk assesment and note the reference number and initial.

Reference number: _____ Initial: _____

Prepare powders:

Weigh powders. ☐

Mix powders in pestle and mortar ☐

Must be done in a fume cupboard.

Weight of chemicals

Boron: _____

Barium oxide: _____

Iron(II/III)oxide: _____

Glycerol: _____

Total: _____

Form a pellet using the press and die. ☐

Pellet formed with pressure of: _____

Place pellet in an alumina boat. ☐

Insert pellet into furnace:

Make sure furnace is cool before opening.

Use the wooden ruler to carefully push and place:

The boat 270mm inside the inner tube. ☐

The inner tube 300mm inside the external tube. ☐

Insert the heat shields, and seal the tube with the end plates. ☐

Turn on the power to the furnace and the MFC. ☐

Initial furnace temperature: _____

Check that the Argon gas line is open. ☐

Open valves: _____

Closed valves: _____

DO NOT MAKE COPIES OF THIS DOCUMENT

Programme the PID. ☐ Programme uesd:

Programme MFC. ☐ Programme used:

At what time will the gas lines have to be altered.

Start the experiment. ☐ Start time: _____
predicted end time: _____

Change the gas valves so the reducing gas is used. ☐ Open valves: _____
Closed valves: _____

Once the furnace has cooled:

Shut off the gas. ☐ Temperature at end of experiment: _____

Turn off power. ☐ End time: _____

Remove the sample.

Place sample in labelled container. ☐ Mass of product: _____

Quality assurance

Take two images of the sample using the optical microscope in the laboratory.
Use a magnification of x1000 in bright field and darkfield with a low camera zoom.
Atatch the images to this document.

THE UNIVERSITY of York

INTERNAL WASTE TRANSFER NOTE

SECTION A. DESCRIPTION OF WASTE

A1. Please describe the waste being transferred.

SECTION B. DESCRIPTION OF WASTE CONTAINERS (*Including any Packaging, Quantities and Volumes*)

B1. Please describe how the waste is contained including the volume and weight.

SECTION C. DESCRIPTION OF THE HAZARDS ASSOCIATED WITH THIS WASTE

C1. Please provide a brief description of the hazards associated with this waste including any compatibility restrictions.

SECTION D. LOCATION OF WASTE PRODUCTION *(To include Department, Building, Room Number etc.)*

D1. Please describe the location and process where the waste has been produced.

SECTION E. CONTACT DETAILS OF THE PERSON HOLDING THE WASTE (TRANSFEROR) THE PROCEDURE

E1. Name		E2. Telephone	
E3. Email Address	york.ac.uk	E4. Date	
E5. Time		E6. Signature	
E7. Departmental Reference or Serial Number			

SECTION F. CONTACT DETAILS OF THE PERSON COLLECTING/RECEIVING THE WASTE (TRANSFEREE)

F1. Name		F2. Telephone	
F3. Email Address	york.ac.uk	F4. Date	
F5. Time		F6. Signature	
F7. Departmental Reference or Serial Number			

SECTION G. WASTE TRANSFER

G1. Department		G2. Location	
G3. Date		G4. Time	
G5. Comments /Notes			

Note. **Waste Transferor to retain a copy of this Internal Waste Transfer Note once the Waste Transferee has accepted the waste and the waste transfer is complete. Copies of Internal Waste Transfer Notes are to be retained for 3 years.**

Reference Number: ……

Nanosystems risk assessment form.

This form should be completed before any work is undertaken in the nanosystems laboratory. A new form should be filled out for every different procedure that will be carried out in the lab. This form is to be filed in the lab for future reference it is recommended that each student keeps a copy for their own reference.

The reference Number at the top of this page should consist of the individuals' initials (in capitals) and a three digit number starting at 001 and rising consecutively for each risk assessment completed.

Name of individual:

The materials that will be used:

The equipment that will be used:

Please note the location at which the work will be done. Note any specific reasons why:

Any specific risk to you or others who may be working in the area at the same time or afterwards:

Please indicate the steps will you take to minimise the risks involved:

Give a brief description of the work including its purpose and how the final product will be used:

Initial

- I confirm I have received and have read and understood all the materials safety data sheets (MSDS) for all materials involved in my work. …….
- I confirm that there are no less hazardous materials that can be used …….
- I confirm that I have received training in how to handle the materials that I will be using, and understand the dangers associated with each material. …….
- I confirm that I have received training in how to use all of the equipment necessary for me to complete my work, and understand the dangers associated with each piece of equipment. …….

Signature: Date:

Countersigned:

Bibliography

[1] *The Oxford English Dictionary*. Oxford University Press, 2009.

[2] Younan Xia, Peidong Yang, Yugang Sun, Yiying Wu, Brian Mayers, Byron Gates, Yadong Yin, Franklin Kim, and Haoquan Yan. One-dimensional nanostructures: Synthesis, characterisation and applications. *Advanced Materials*, 15:353, 2003.

[3] Jifa Tian, Chao Hui, Lihong Bao, Chen Li, Yuan Tian, Hao Ding, Chengmin Shen, and Hong jun Gao. Patterned boron nanowires and field emission properties. *Applied Physics Letters*, 94:083101, 2009.

[4] L Calbri, N Pugno, W Ding, and R S Ruoff. Resonance of curved nanowires. *Journal of Physics: Condensed Matter*, 18:s2175, 2006.

[5] Yu Huang, Xiangfeng Duan, Yi Cui, Lincoln J. Lauhon, Kyoung-Ha Kim, and Charles M. Lieber. Logic gates and computation from assembled nanowire building blocks. *Science*, 294:1313, 2001.

[6] Bin Wu, Andreas Heidelberg, John J. Boland, John E. Sader, XiaoMing Sun, and YaDong Li. Microstructure-hardened silver nanowires. *Nano Letters*, 6:468, 2006.

[7] Xingjun Wang, Jifa Tian, Tianzhong Yang, Lihong Bao, Chao Hui, Fei Liu, Chengmin Shen, Changzhi Gu, Ningsheng Xu, and Hongjun Gao. Single crystalline boron nanocones: Electric transport and field emission properties. *Advanced Materials*, 19:4480, 2007.

[8] Zheng Wei Pan, Zu Rong Dai, and Zhong Lin Wang. Nanobelts of semiconducting oxides. *Science*, 291:1947, 2001.

[9] Guo-Bin Shan and George P Demopoulos. The synthesis of aqueous-dispersible anatase tio2 nanoplatelets. *Nanotechnology*, 21:025604, 2010.

[10] Haoquan Yan, Justin Johnson, Mat Law, Rongrui He, Kelly Knutsen, Juan R. McKinney, Johnny Pham, Richard Saykally, and Peidong Yang. Zno nanoribbon microcavity lasers. *Advanced Materials*, 15:1907, 2003.

[11] C.N.R.Rao, F.L. Deepak, Gautam Gundiah, and A. Govindaraj. Inorganic nanowires. *Progress in Solid State Chemistry*, 31:5, 2003.

[12] Ali O. Sezer and J. I. Brand. Chemical vapour deposition of boron carbide. *Materials science and Engineering*, B79:191, 2001.

[13] Hugh D. Young and Roger A. Freedman. *University Physics with modern physics 11th Edition*, page 1607. Addison Wesley, 2004.

[14] H. Hofmeister. Fivefold twinned nanoparticles. *Encyclopedia of Nanoscience and Nanotechnology*, 3:431, 2004.

[15] M Audronis, O Jimenez, and A Mathews. The morphology and structure of pvd zrn- cu thin films. *Journal of Physics D: Applied Physics*, 42:085308, 2009.

[16] L. Guo, R. N. Sing, and H. J. Kleebe. Growth of boron-rich nanowires by chemical vapour deposition (cvd). *Journal of Nanomaterials*, 2006:1, 2006.

[17] Yingjiu Zhang, Hiroki Ago, Motoo Yumura, Satodhi Ohshima, Kunio Uchida, Toshiki Komatsu, and Sumio Iijima. Study of the growth of boron nanowires synthesized by laser ablation. *Chemical Physics Letters*, 385:177, 2004.

[18] Atsushi Kuwabara, Shin ichi Kuroda, and Hitoshi Kubota. Preperation of a cvd thin film by an atmospheric pressure low temperature surface discharge plasma torch. *Plasma Sources Science and technology*, 15:328, 2006.

[19] Yunho Baek, YongHwan Ryu, and Kijung Yong. Structural characterisation of β-sic nanowires synthesized by direct heating method. *Materials Science and Engineering*, 26:805, 2006.

[20] M. Zenotchkine, R. Shuba, and I-Wei Chen. Liquid-phase growth of small crystals for seeding α -sialon ceramics. *Journal of the American Ceramic Society*, 87:1040, 2004.

[21] Yu Cui, Lincoln J. Lauhonand Mark S Gudiksen, Jianfang Wang, and Charles M. Lieber. Diamater-controlled synthesis of single-crystal silicon nanowires. *Applied Physics Letters*, 78:2214, 2001.

[22] Limin Cao, Jing Liu, Cunxiao Gao, Yancun Li, Xiaodong Li, Y Q Wang, Z Zhang, Qiliang Cui, Guangtian Zou, Liling Sun, and Wenkui Wang. Synthesis of well-aligned boron nanowires and their structural stability under high pressure. *Journal of Physics: Condensed Matter*, 14:11017, 2002.

[23] Y.Q. Wang, X.F. Duan, L.M.Cao, and W.K. Wang. One-dimensional growth mechanism of amorphous boron nanowires. *Chemical Physics Letters*, 359:273, 2002.

[24] Q. Yang, J. Sha, L. Wang, z. Su, x. Ma, J. Wang, and D Yang. Morphology and diameter controllable synthesis of boron nanoiewrs. *Journal of Material Science*, 41:3547, 2006.

[25] Renzhi Ma and Yoshio Bando. High purity single crystalline boron carbide nanowires. *Chemical Physics Letters*, 364:314, 2002.

[26] Carolyn Jones Otten, Oleg R. Lourie, Min-Feng Yu, John M. Crowlay, Mark J. Dyer, Rodney S. Ruoff, and William E. Buhro. Crystaline boron nanowires. *American Chemical Society*, 124:4564, 2002.

[27] Minghe Cao, Jun Jiang, Hanxing Liu, and Jun Yuan. A simple method to prepare boron suboxide fibres. *Journal of Electroceramics*, 17:817, 2006.

[28] Jun Jiang, Minghe Cao, Yuekui Sun, Peiwen Wu, and Jun Yuan. Star-shaped cyclic-twinning nanowires. *Applied Physics Letters*, 88:163107, 2006.

[29] Xin Fu, Jun Jiang, Chao Liu, Zhi-Yang Yu, Steffan Lea, and Jun Yuan. Re-entrant-groove-assisted vls growth of boron carbide five-fold twinned nanowires. *Chinese Physical Letters*, 28:086110, 2009.

[30] Jun Jiang. Phd thesis. *Tsinghua University, Beijing*, 2007.

[31] T. Hahn and H. Klapper. *International Tables for Crystallography, D*. Dordrecht Kluwer, 2003.

[32] Harry L. Yakel. The crystal structure of a boron-rich boron carbide. *Acta Crystallographica*, B31:1797, 1975.

[33] Xin Fu, Jun Jiang, Wenzheng Zhang, and Jun Yuan. Incoherent structural relaxation of fivefold twinned nanowires. *Applied Physics Letters*, 93:043101, 2008.

[34] C.W. Oatley. The early history of the scanning electron microscope. *Journal of applied physics*, 53:R1, 1982.

[35] David B. Williams and C. Barry Carter. *Transmission Electron Microscopy*. Springer, 1996.

[36] D. Shindo and T. Oikawa. *Analytical Electron Microscopy for Materials Science*. Springer, 2002.

[37] Shoushan Fan, Jien Cao, Haiyan Dang, Qian Gu, and Jianhong Zhao. Growth of semiconductor nanowires on iron-patterned silicon substrates. *Materials Science and Engineering C*, 15:295, 2001.

[38] Paola Favia, Tiziana Stoto, Michel Carrard, Pierre-Andre Stadelmann, and Libero Zuppiroli. Order and disorder in boron phases. *Microscopy Microanalysis Michrostructures*, 7:225, 1996.

[39] S. Dierks. Msds for iron boride. 1990.

[40] Yung Joon Jung, Bingquing Wei, Robert Vajtai, and Pulickel M. Ajayan. Mechanism of selective growth of carbon nanotubes on sio_2/si patterns. *Nano Letters*, 3:561, 2003.

[41] Francesco Mauri, Nathalie Vast, and Chris J. Pickard. Atomic structure of icosahedral b4c boron carbide from first principles analysis of nmr spectra. *Physical Review Letters*, 87:085506, 2001.

[42] Lianne Scrutton. Mphys thesis. *The University of York*, 2009.

[43] S. Ramana Murthy. Elastic properties of boron carbide. *Journal of materials science letters*, 4:603, 1985.

[44] Cheng-Lun Hsin, Wenjie Mai, Yudong Gu, Yifan Gao, Chi-Te Huang, Yuzi Liu, Lih-Juann Chen, and Zhong-Lin Wang. Elastic properties ond buckling of silicon nanowires. *Advanced Materials*, 20:3919, 2008.